universität wien

MASTERARBEIT | MASTER'S THESIS

Titel | Title

Impact of time-averaging on the calculation of photovoltaic power output on the basis of climate simulations

verfasst von | submitted by

Patricia Schluschanek BSc

angestrebter akademischer Grad | in partial fulfilment of the requirements for the degree of

Master of Science (MSc)

Wien | Vienna, 2025

Studienkennzahl lt. Studienblatt | Degree programme code as it appears on the student record sheet:	UA 066 614
Studienrichtung lt. Studienblatt | Degree programme as it appears on the student record sheet:	Masterstudium Meteorology and Climate Science
Betreut von | Supervisor:	Univ.-Prof. Dr. Aiko Voigt

Abstract

In this thesis, I study the effects of time averaging on the calculation of potential photovoltaic (PV) power yield. Thus I analysed the spread of several CMIP6 models with an AMIP and an AMIP-p4K configuration and daily mean time resolution and compared it to ICON-ESM climate simulations with a native time resolution of 15 minutes.

The changes in potential PV power yield under climate change have been previously examined in a number of publications. The most frequently used daily mean input data for the calculation of the time-dependent potential PV power yield posed a significant restriction due to the filtering out of lows and highs in power production. Most studies found changes in the single-digit percentage range. For the purpose of my thesis, I use ICON-ESM simulations with a temporal resolution of 15 minutes and averaged the input variables across several periods, with the longest being 24 hours, prior to the calculation of the potential PV power yield. The results were then compared. My findings reveal that the time averaging of daily mean data led to an overestimation of relative percentage of 6.3% on a global scale. The absolute overestimation caused by time averaging during months with the highest and lowest PV power generation was found to be +1.5% and +0.1%, respectively. Furthermore, seasonal variations were identified across Europe, Austria and Vienna. The multi-model and daily mean potential PV power yield for eight GCMs with an AMIP configuration was determined to be 19.20%. Globally, the daily multi-model mean potential PV power yield calculated with seven GCMs using an AMIP-p4K configuration decreased slightly compared to the AMIP models (18.5%), which is in agreement with several previous publications. Since previous publications have found changes in potential PV power yield that are within the range of my calculated overestimation, it is clear that daily mean data sets are not suitable for PV power estimation.

Zusammenfassung

In dieser Arbeit untersuche ich die Auswirkungen der zeitlichen Mittelung auf die Berechnung des potentiellen photovoltaischen (PV) Stromertrags. Dazu analysierte ich die Verteilung verschiedener CMIP6 Modelle mit einer AMIP und einer AMIP p4K Konfiguration und einer mittleren täglichen Zeitauflösung und vergleiche sie mit ICON-ESM Klimasimulationen mit einer nativen Zeitauflösung von 15 Minuten.

Die Veränderungen des potenziellen PV-Stromertrags unter dem Einfluss des Klimawandels wurden bereits in einer Reihe von Veröffentlichungen untersucht. Die für die Berechnung des zeitabhängigen potenziellen PV-Stromertrages am häufigsten verwendeten Tagesmittelwerte stellten eine erhebliche Einschränkung dar, da Tief- und Hochpunkte der Stromproduktion herausgefiltert wurden. Die meisten Studien fanden Veränderungen im einstelligen Prozentbereich. Für meine Arbeit habe ich ICON-ESM-Simulationen mit einer zeitlichen Auflösung von 15 Minuten verwendet und die Eingangsvariablen vor der Berechnung des potenziellen PV-Stromertrags über mehrere Zeiträume gemittelt, wobei der längste 24 Stunden betrug. Die Ergebnisse wurden dann miteinander verglichen. Meine Ergebnisse zeigen, dass die zeitliche Mittelung von Tagesmittelwerten zu einer relativen Überschätzung von 6,3% auf globaler Ebene führte. Die absolute Überschätzung, die durch die zeitliche Mittelung in den Monaten mit der höchsten und niedrigsten PV-Stromerzeugung verursacht wurde, lag bei +1,5% bzw. +0,1%. Darüber hinaus wurden saisonale Schwankungen in ganz Europa, Österreich und Wien festgestellt. Der multimodale und tägliche Mittelwert des potenziellen PV-Stromertrags für acht GCMs mit einer AMIP-Konfiguration wurde mit 19,2% ermittelt. Der mit sieben GCMs und einer AMIP-p4K-Konfiguration berechnete mittlere tägliche potenzielle PV-Energieertrag ging im Vergleich zu den AMIP-Modellen leicht zurück (18.5%), was mit mehreren früheren Veröffentlichungen übereinstimmt. Da in früheren Veröffentlichungen meist Änderungen des potenziellen PV-Stromertrags im einstelligen Prozentbereich festgestellt wurden, die im Bereich der von mir berechneten Überschätzung liegen, ist klar, dass Tagesmittelwerte für die Abschätzung der PV-Leistung ungeeignet sind.

Contents

1 Introduction

My master's thesis is part of the "KlipPer" project, a joint initiative of the University of Vienna and the Austrian Institute of Technology (AIT). The acronym "KlipPer" stands for *Klimawandelprojektion und Photovoltaikertrag*, which translates to *Climate change projections and photovoltaic power yield*. The objective of this project is to develop novel methods for integrating global climate simulations with photovoltaic yield models.

The generation of photovoltaic (PV) energy is influenced by a number of factors, including solar irradiance, ambient temperature and wind conditions. These parameters are subject to change under climate change, which can affect PV energy production. Irradiance reaching the Earth's surface is a primary driver of energy production.

Several studies, including Crook et al. (2011), Panagea et al. (2014), Jerez et al. (2015), Feron et al. (2021) and Baur et al. (2024), calculated a photovoltaic power potential (PV_{pot}). The input variables are the *down-welling short-wave radiation on the surface for the grid cell* ($RSDS$), the *surface temperature* in degrees Celsius (TAS) and the *near-surface wind speed* (VWS). PV_{pot} compares PV power output to ideal output under standard conditions:

$$PV_{pot}(t) = P_R(t)\frac{RSDS(t)}{RSDS_{STC}}, \tag{1}$$

where $RSDS_{STD} = 1.000 Wm^{-2}$ is the *down-welling short-wave radiation on the surface under standard conditions* and P_R is the *performance ratio* which describes the cells efficiency depending on the cell temperature:

$$P_R(t) = 1 + \beta(T_{cell}(t) - T_{STC}), \tag{2}$$

where $T_{STD} = 25°C$ is the *cell temperature under standard conditions* and T_{cell} is the *actual cell temperature*. The coefficient $\beta = -0.005\ °C^{-1}$ was determined empirically by Tonui et al. (2007). The cell temperature is dependent on $RSDS$, TAS and VWS:

$$T_{cell}(t) = c_1 + c_2 \cdot TAS(t) + c_3 \cdot RSDS(t) + c_4 \cdot VWS(t). \tag{3}$$

The coefficients $c_1 = 4.3\ °C$, $c_2 = 0.943$, $c_3 = 0.028\ °Cm^2W^{-1}$, $c_4 = -1.528\ °Csm^{-1}$ were determined by Tamizhmani et al. (2003) and consist of averages of the coefficients for multiple photovoltaic cells. $RSDS$ and TAS heat up the cell, while VWS has a cooling effect.

Should the actual cell temperature exceed standard conditions, the performance ratio is known to decrease, thereby reducing the PV_{pot}. The highest PV_{pot} can be achieved with low temperatures and high radiation.

If ambient conditions are equal to standard conditions $PV_{pot} = 1$ or 100%. The result of this method is a potential which means that it is not influenced by external disturbances of the panel itself, e.g. dust or snow cover, wildlife, anthropogenic influences, etc.

As demonstrated in Figure 1a, the amount of irradiance reaching a solar panel has a large effect on the current output of the cells. It is evident from the figure that as irradiance levels rise, the current output of the PV panel also increases, reaching a maximum power point. Solar panels are generally operated close to this maximum power point in order to maximise energy production.

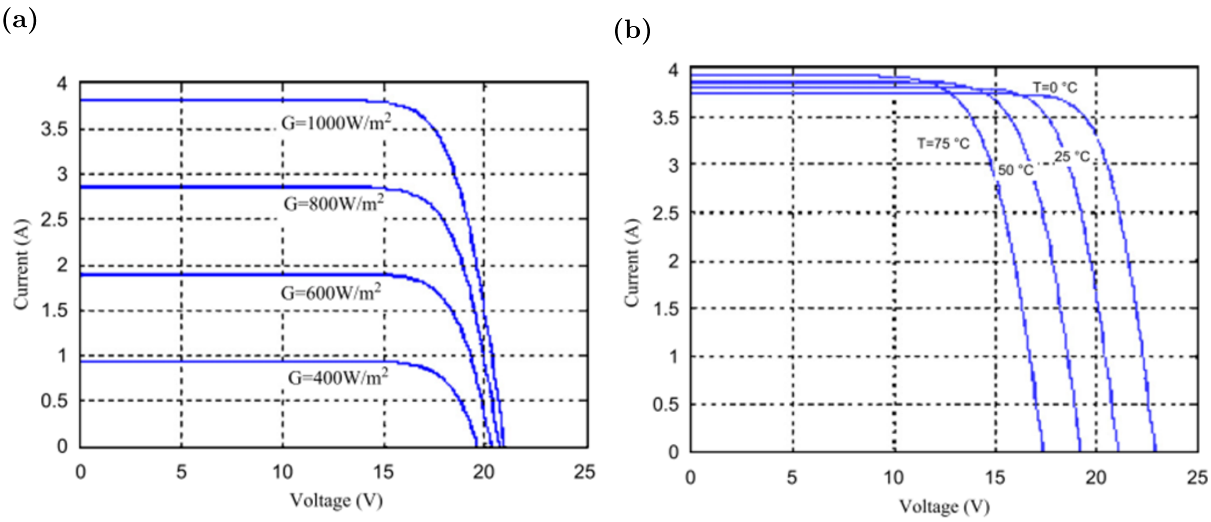

Figure 1: Taken from Chenni et al. (2007). Figures show the effects of a) irrandiance (G) and b) temperature (T) on current-voltage characteristic curve. The x-axes represent the voltage in Volts, the y-axes respresent the current in Ampere.

It is known that a negative correlation exists between the temperature and the PV power output. As demonstrated in Figure 1b, the maximum voltage output of the PV panel rises with decreasing air temperature. Increasing temperatures result in decreased voltages, leading to a reduced maximum power point (Chenni et al., 2007). Another challenge for PV power generation is that irradiance absorbed by the ground can lead to an increase in surface temperature (Feron et al., 2021; Panagea et al., 2014).

Manufacturers of solar panels use the term *nominal power* or *installed power* to denote the amount of power a device or module is capable of generating under standard conditions (E.ON Energie Deutschland GmbH, 2025). To calculate the total wattage produced one has to multiply the PV_{pot} with the *nominal power*.

Several studies analysed the changes in PV_{pot} due to climate change and used input data with different time resolutions. One of the earlier studies on the topic by Crook et al. (2011) used two CMIP3 models to draw comparisons between a baseline climatology (1980-1999) and changes simulated for the year 2100. They used an IPCC emissions scenario describing a future with very rapid economic growth and a world population that peaks in the middle of the century and declines thereafter, as well as the introduction of new and more efficient technologies[1]. While the emission of greenhouse gases and sulphate aerosols was specified, other aerosol species were open to the different modelling groups. The datasets were temporally resolved to monthly means. The authors' primary focus was on multiple regions characterised by the presence of substantial solar power facilities.

[1] IPCC emissions scenario SRES A1B10

The authors concluded that PV_{pot} is strongly dependent on location. As illustrated in Figure 2, the study found that PV_{pot} is likely to increase by a few percent in Europe and China, show negligible change in Algeria and Australia, and decrease by a few percent in the western USA and Saudi Arabia. The authors found that a decrease of PV_{pot} occurs in regions with a decrease in irradiance and an increase in temperature.

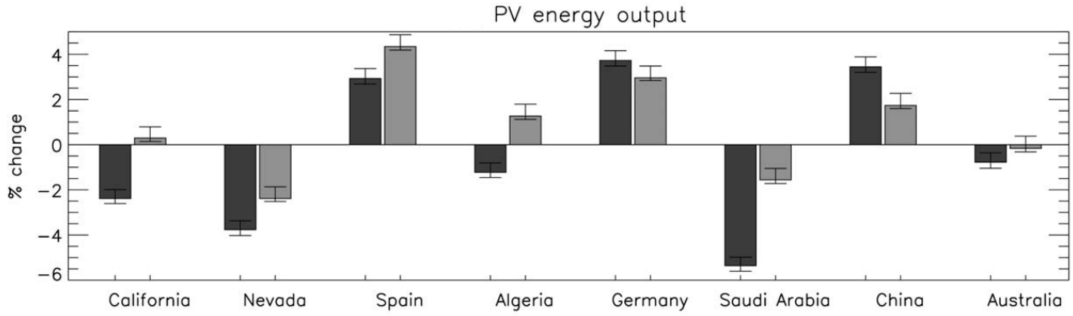

Figure 2: Taken from Crook et al. (2011). Relative change in PV energy output for different regions for two CMIP3 models (HadGEM1 in dark grey, HadCM3 in light grey). Vertical error bars show the uncertainty stemming from the different predicted temperature changes in the models.

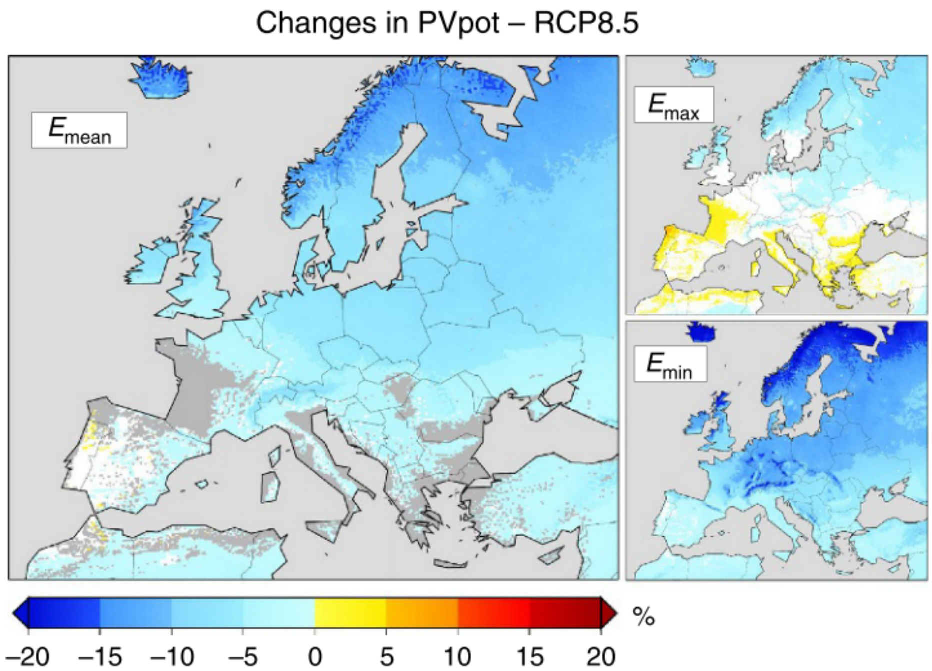

Figure 3: Taken from Jerez et al. (2015). Climate change projections under RCP8.5. Changes projected in the mean values of PV_{pot} under the RCP8.5 at the end of this century (2070-2099 versus 1970-1999) obtained from the ensemble mean (E_{mean}), the ensemble maximum (E_{max}) and the ensemble minimum (E_{min}) over land. Values in E_{max} and E_{min} are coloured only if they are significant within their corresponding ensemble member. E_{mean} values are coloured only if they are robust, in white if they are negligible and in grey if they are uncertain.

In a study by Jerez et al. (2015), the authors compared an ensemble of 10 regional and global climate models from the EURO-CORDEX project for the period from 1970 to 2099, analysing two climate scenarios (RCP4.5 and RCP8.5). As displayed in Figure 3, the study revealed an absolute change in PV_{pot} of approximately 10% under the RCP 8.5 scenario, with the exception of specific regions exhibiting negligible or uncertain results, such as southeastern Iberia, western France, and certain coastlines from Italy to Turkey. The maximum changes were found to be in the range of ±20 %. Under the RCP4.5 scenario, global signals were found to be distributed in a similar manner, yet reduced by a factor of two compared to the RCP8.5 scenario.

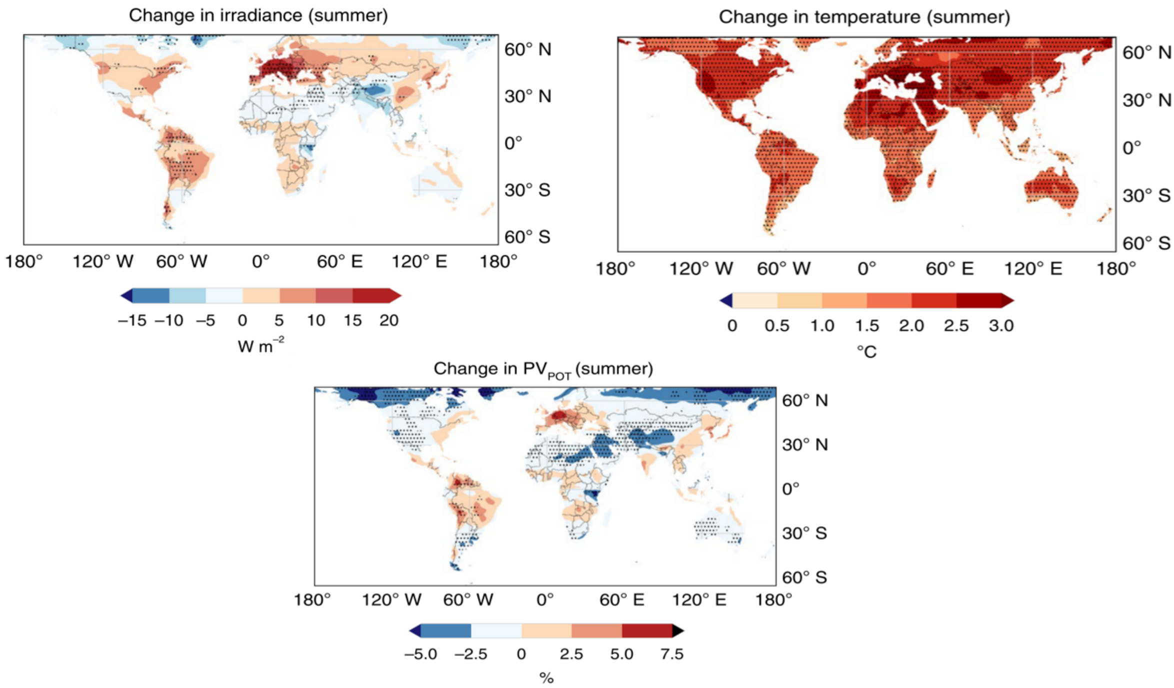

Figure 4: Taken from Feron et al. (2021). Changes during each hemisphere's summer months from 1961-1990 to 2036-2065 for RCP 4.5 in a multi-model mean (CMIP5). Upper left: irradiance, upper right: surface temperature, bottom: potential PV yield. Dotted areas mark robust results (85% of the models agree).

Figure 4 shows results by Feron et al. (2021). The authors analysed changes in PV_{pot} due to climate change with the previously introduced method. They compared a climatology for the period from 1961 to 1990 to a RCP4.5 climate scenario from 2036 to 2065. They used daily mean input data from seven CMIP5 models for both periods. Figure 4 illustrates the absolute changes that occurred during the summer months in both hemispheres. The authors found moderate changes in PV_{pot} across the Atacama Desert of +3%, eastern China, southeastern Asia and the northeastern United States of +2%, southeastern Australia, northwestern Africa and southwestern United States of -2% and central Asia of -3%. Large changes in PV_{pot} were found on the Arabian peninsula with a decrease of 4% and in central Europe with an increase of 5%. Positive changes were mostly caused by an increasing irradiance, while negative changes were due to increasing temperatures. The authors found that an increase of temperature does not only affect the PV cells performance but also negatively affect the irradiance by influencing clouds and aerosols. The large changes across Europe are mostly driven by changes in irradiance while the Arabian Peninsula experiences only a slightly decreasing irradiance but a stronger increase in temperature which causes the PV_{pot} to decrease.

The method, that is used by the previously discussed studies and my thesis, does have a number of shortcomings. There are several uncertainties with unknown effects on the calculation of PV_{pot}.

First, the coefficient employed in the calculation of the performance ratio is subject to a considerable degree of inconsistencies. It was determined by Tonui et al. (2007) through empirical means to be $\beta = -0.0063°C^{-1}$. Crook et al. (2011), Feron et al. (2021) and Jerez et al. (2015) used the coefficient $\beta = -0.005°C^{-1}$ without further explanation. Skoplaki et al. (2009) derived a value of $\beta = 0.0045°C^{-1}$. In contrast, Tonui et al. (2007) determined the original coefficient through empirical means for a panel located in Greece, with a fitting tilt for the region. The uncertainty this brings for the calculations of other regions is currently not known.

Further, the coefficients used in the calculations of the cell temperature show uncertainties because they were established using now outdated equipment. They were determined empirically in 2003 for several different photovoltaic modules available at the time by Tamizhmani et al. (2003) as part of a study at the Photovoltaic Testing Laboratory at Arizona State University. The study encompassed 22 photovoltaic modules of six distinct types, the majority of which are still commonly utilised PV module types in the present day. The determined coefficients were then averaged for all 22 modules. The application of six distinct working methods for PV module resulted in considerable variations, as illustrated in Table 1.

Table 1: Coefficients for the calculation of the cell temperature (Tamizhmani et al., 2003).

	$\mathbf{c_1}$ [°C]	$\mathbf{c_2}$	$\mathbf{c_3}$ [$\mathbf{°Cm^2W^{-1}}$]	$\mathbf{c_4}$ [$\mathbf{°Csm^{-1}}$]
Average	4.318	0.943	0.028	-1.528
Minimum	2.700	0.914	0.022	-1.770
Maximum	6.100	0.979	0.033	-1.288
Spread	3.400	0.065	0.011	0.482

A subsequent limitation of the present method is that it considers surface down-welling short-wave radiation exclusively for its calculation, while disregarding the distinction between direct and diffuse radiation. It is noteworthy that the majority of preceding studies used datasets for which this distinction was not available, for instance, CMIP data. This distinction is only pertinent for panels with a tilt, which represents a further overlooked detail of this method, given that surface plane installation of the panels is not generally the most efficient method.

A significant restriction of previous studies is that the majority of calculations are based on daily mean (Panagea et al., 2014; Jerez et al., 2015; Feron et al., 2021) or monthly mean (Crook et al., 2011) datasets. Given that the input variables are time-dependent, it follows that the equations are also time-dependent. The potential PV power output during nighttime drops to zero due to the lack of radiation, so time averaging over the whole day filters out the daytime peaks. Furthermore, temperature peaks are also subject to averaging. High irradiance is often linked to high temperatures, which in turn increases cell temperature and therefore reduces PV_{pot}. PV_{pot} may be overestimated when high surface temperatures are filtered out, due to the absence of dampening effects from the cell temperature. Additionally, daily data is suboptimal for PV calculation models, which necessitate high temporal resolution, given the rapid and frequent changes in radiation.

2 Research Question

The prevailing methodology for photovoltaic power yield calculations in the field of climate study is reliant upon time-dependent input variables (see section 1, page 6). Previous studies (section 1, page 7) used daily mean or even monthly mean data to calculate the potential photovoltaic power yield, a practice that introduces unknown uncertainties. Daily or monthly mean data, whilst convenient, is not ideal for PV yield estimation, which requires high temporal resolution, due to the rapid and frequent changes in irradiance and further temperature and wind speed. The central objective of my thesis is to analyse the potential errors (see section 1, page 10) that arise from using time-averaged datasets.

My research question formulated for this study is as follows:

> **What is the error in potential photovoltaic power yield due to the use of time-averaged data?**

In order to answer my research question, I compare the potential photovoltaic power yield calculated with input data at eight different temporal resolutions using a climate simulation (ICON-ESM) with high temporal resolution output. The calculation is done with a method commonly used in previous studies (see section 1, page 6) in order to get a comparison with the mentioned studies. Furthermore, deviations from time-averaging are compared to those determined using CMIP6 models with daily mean data.

3 Methodology

To answer my research question, I first calculated PV_{pot} using the common approach that has been used in previous publications (see section 1, page 6) for seven CMIP6 models with a daily mean time resolution and determined the spread of the models. I then compared calculations of PV_{pot} using the daily maximum and daily mean of the input variables from two ICON-ESM simulations. Finally, I calculated PV_{pot} for different time resolutions using two ICON-ESM simulations. This was done in order to study the magnitude of the uncertainties due to time-averaging.

The ICON-ESM simulation is characterised by a temporal resolution of 15 minutes, a feature that makes it possible to see decreases of PV_{pot} due to elevated temperatures or peak performances resulting from high radiation.

3.1 CMIP6 Models

In order to replicate the findings of previous studies, I analysed seven CMIP6 models. CMIP, an acronym for the *Coupled Model Intercomparison Project*, is an international project whose objective is to improve understanding of past, present and future climate using climate models. Since every model uses slightly differing input parameters and is structured differently, results vary for every climate simulation. More than 50 modelling centres around the world participated in the sixth phase of CMIP, called CMIP6. CMIP6 represents the latest phase of CMIP, while the development of CMIP7 is still in its early stages (Coupled Model Intercomparison Project IPO, 2024). For the purposes of this analysis, I chose models for which the input parameters were available in daily mean time resolution. Coincidentally, a range of diverse modelling centres around the world were used (see Table 2).

I selected the de facto standard experimental protocol for global atmospheric general circulation models (AGCMs) - the *Atmospheric Model Intercomparison Project* (AMIP) - for all CMIP6 models. Since 1990, its objective has been to facilitate analysis of atmospheric processes by focusing on the atmospheric model. The AMIP simulation has prescribed sea surface temperatures and sea ice concentrations derived from monthly averaged observations, prescribed CO_2 concentrations and solar constant (Gates et al., 1999).

To analyse the effects of rising temperatures I used an additional six CMIP6 models with an AMIP-p4K simulation (see Table 2). The AMIP-p4K configuration is derived from the AMIP model, but with a uniform increase of 4 Kelvin in sea surface temperatures. My objective is to verify the occurrence of shifts in PV_{pot} attributable to rising temperatures. It is not feasible to make assertions regarding the magnitude of changes in PV_{pot} due to climate change with this configuration, as this would require a coupled atmosphere-ocean model, neither is it a research objective of my thesis.

Table 2: CMIP6 models used. From left to right: model name, modelling centre, time span of available data for AMIP and AMIP-p4K.

Model name	Modelling Centre	AMIP	AMIP-p4K
BCC-CSM2-MR	**BCC** (Beijing Climate Center)	1979-01-01 until 2014-12-31	1979-01-01 until 2014-12-31
CESM2	**NCAR** (National Center for Atmospheric Research)	1950-01-01 until 2015-01-01	1979-01-01 until 2013-01-01
IPSL-CM6A-LR	**IPSL** (Institut Pierre-Simon Laplace)	1979-01-01 until 2014-12-31	1979-01-01 until 2014-12-31
MIROC6	**MIROC** (Atmosphere and Ocean Research Institute (AORI), Centre for Climate System Research - National Institute for Environmental Studies (CCSR-NIES) and Atmosphere and Ocean Research Institute (AORI))	1979-01-01 until 2014-12-31	1979-01-01 until 2014-12-31
MPI-ESM1-2-LR	**MPI-M AWI** (Max Planck Institute for Meteorology (MPI-M), AWI (Alfred Wegener Institute))	1979-01-01 until 2014-12-31	N/A
MRI-ESM2-0 4	**MRI** (Meteorological Research Institute, Japan)	1979-01-01 until 2014-12-31	1979-01-01 until 2014-12-31
TaiESM1	**AS-RCEC** (Research Center for Environmental Changes)	1979-01-01 until 2014-12-31	1979-01-01 until 2010-12-31

For all datasets I chose the first ensemble member with the variant-ID r1i1p1f1. The variant-ID provides a comprehensive description of the configuration of the simulation. The subsequent number following a letter denotes the specified setting, with r denoting realization, i initialization, p physics, and f forcing (Taylor et al., 2012). All models provide daily mean data for the three input variables $RSDS$, TAS and VWS (see section 1, page 6).

My analysis considered a 30-year period (from 1980 to 2010), a time frame determined by the availability of the necessary data. Given the unfeasibility of solar energy plants on the free ocean surface, a land mask was applied to all datasets. To do so, the land area fractions of each model were converted into land masks and applied to the respective input datasets. The 13 datasets (7 AMIP simulations and 6 AMIP-p4K simulations) were then regridded to a resolution of 320 x 160 grid cells on a regular longitude x latitude grid, which equates to 1.125 x 1.125 degrees. For all processing of the CMIP6 datasets I used the command line tool CDO (Climate Data Operators) by Schulzweida (2023).

3.2 ICON-ESM simulation

I made a comparison between the CMIP6 models and ICON-ESM simulations, with the ICON-ESM simulations being run on the *Vienna Scientific Cluster* (VSC).

The ICON-ESM is a global coupled climate model developed by the *Max-Plank Institute of Meteorology* (MPI), the *Deutscher Wetterdienst* (DWD) and the *Karlsruhe Institute for Technology*, as well as further partner institutions in Germany and Switzerland. The ICON-ESM simulation is based on the ICON-framework. For the purposes of my thesis, I conducted an ICOsahedral Non-hydrostatic-ESM V1.0 simulation, which is the first version of the *ICON-Earth System Model*. The model combines the ICON-O and ICON-A models for ocean and atmosphere components respectively, with the ICON-Land simulation and a scheme for biosphere-atmosphere coupling (JSBACH 4), as well as a revised version of the land model, JSBACH 3. The ICON-ESM output is on an icosahedral grid, a characteristic feature of ICON models, with a horizontal resolution of approximately 160 km and a vertical distribution comprising 47 atmospheric levels. The native temporal resolution is an output at 15-minute intervals; however, the radiation scheme is only called at 90-minute intervals (Jungclaus et al., 2022).

In total I ran two ICON-ESM simulations. Like the CMIP6 models I chose one AMIP and one AMIP-p4K simulation (see section 3.1). I ran both simulations for the time between 1979 and 2010. The year 1979 was not considered for my analysis to avoid spin-up effects. After applying a land mask, I regridded the simulations to a regular longitude x latitude grid with a resolution of 320 x 160 grid cells, which equates to 1.125 x 1.125 degrees. I applied the masks and regridded the data with the command line tool CDO.

3.3 Calculation of PV_{pot}

I calculated PV_{pot} with the previously introduced method (see section 1, page 6) with already time averaged input data and with the native 15-minutes time resolution output from the ICON-ESM simulations. For all calculations of PV_{pot} I used python.

3.4 Time averaging

For my study, I time-averaged all input parameters of all models and excluded leap days.

To compare the daily mean PV_{pot}, I used daily mean input variables. To this end, I averaged the ICON-ESM model parameters to daily mean datasets. The CMIP6 models already had a daily mean time resolution. After selecting the desired region (Global, Europe, Austria or Vienna) and averaging over the whole analysed period or the corresponding season of each year, I calculated the differences for the whole period.

For the comparison of the PV_{pot} calculated from daily maximum and daily mean input data, I averaged the output from the ICON-ESM simulations with a native time resolution of 15 minutes to daily mean and daily maximum data using the command line tool CDO. I calculated PV_{pot} from the daily mean and daily maximum data and made a comparison of the time and seasonal mean.

Finally, I averaged the output variables $RSDS$, TAS and VWS from the ICON-ESM simulations over all considered averaging periods (30 minutes, 1 hour, 3 hours, 4 hours, 6 hours, 12 hours and 24 hours) using the command line tool CDO. I calculated PV_{pot} for every time step of every averaging period using python and selected the desired region (Global, Europe, Austria or Vienna) using CDO. To facilitate a meaningful comparison, I calculated monthly means for the complete time period.

3.5 Averaging over regions

In addition to the global dataset, I selected three regions for further analysis: a wider European area, an area centred over Austria, and Vienna. The geographical area of Europe extends from 35° N to 80° N and from 25° W to 40° E (see Figure 5a). The geographical area of Austria was chosen from 46.22° N to 49.01° N and from 9.32° E to 17.10° E (see Figure 5b). The area of Vienna represents an exception due to its size and the spatial resolution of the datasets. I selected the area encompassing the four nearest grid points to St. Stephen's Cathedral, which is situated in the centre of Vienna at 48.2085° N 16.373° E.

(a)

(b)

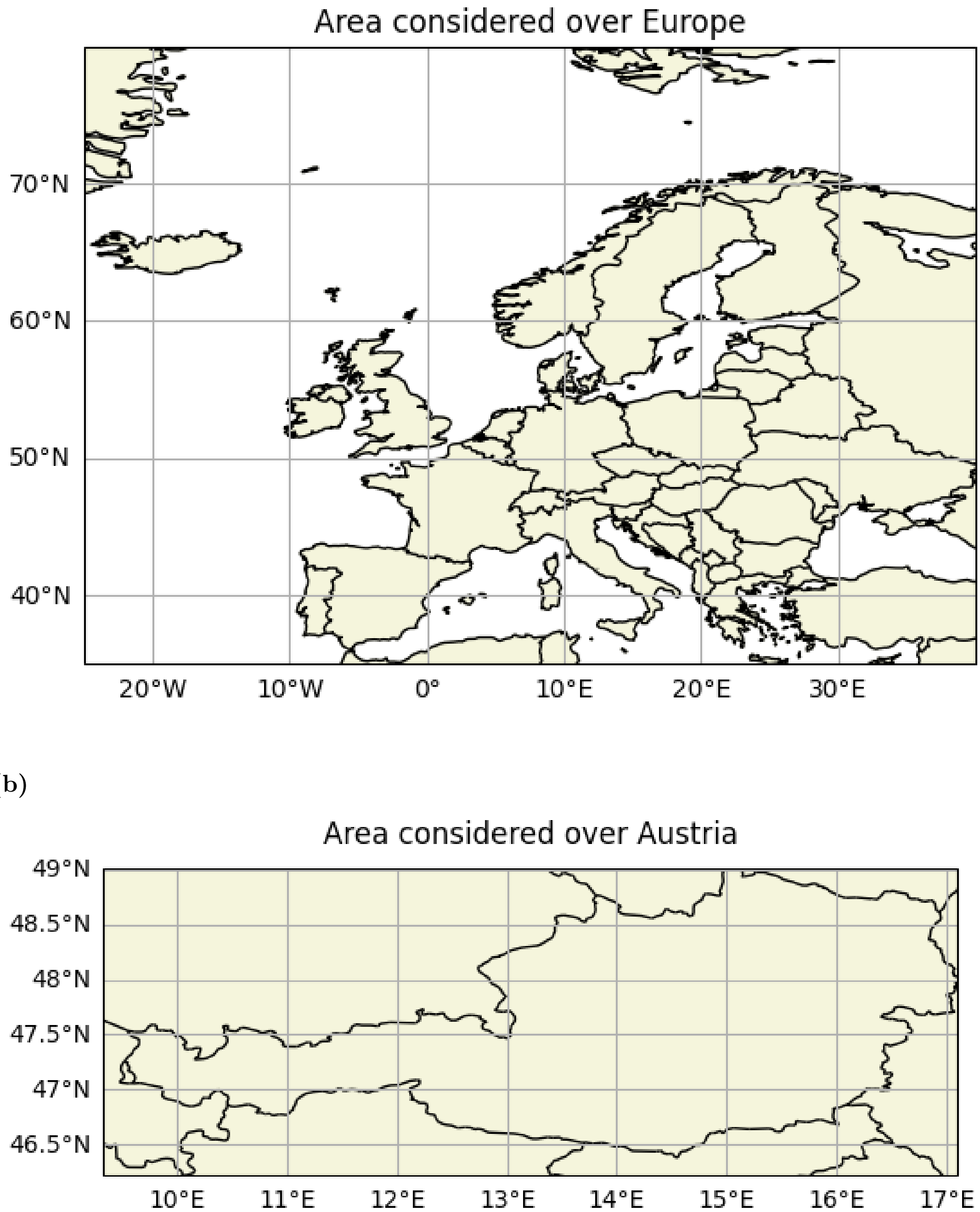

Figure 5: Regional domain selected for the analysis: a) over Europe and b) over Austria.

4 Results and discussion

This chapter presents and discusses the results of my work, the structure of which is as follows: section 4.1 discusses the differences of PV_{pot} calculated with CMIP6 models and two ICON-ESM simulations. Section 4.2 analyses missed peaks in PV_{pot} when using daily mean data. Section 4.3 discusses the effects of using time-averaged data and determines the deviations because of it.

4.1 Differences in PV_{pot} calculated from daily-mean CMIP6 & ICON-ESM models

A number of earlier studies employed daily mean input datasets for their calculations. The objective of this part of my study is to quantify the spread of PV_{pot} calculated with daily mean input data from seven CMIP6 models for the AMIP simulations and six for the AMIP-p4K simulations and an ICON-ESM simulation for each configuration, thereby determining the magnitude of deviations. The spread between the calculations serves as a baseline for my subsequent analysis.

4.1.1 Differences between AMIP and AMIP-p4K simulations

Figure 6a shows the temporal and multi-model mean PV_{pot} of all AMIP models. The global multi-model mean is 19.2%, whilst regional calculations yield a mean PV_{pot} over Europe of 14.3%, 14.4% over Austria, and 14.5% over Vienna. As anticipated, the highest mean PV_{pot} can be seen over the Tropics, with a decline towards the poles.

Figure 6b shows the temporal and multi-model mean PV_{pot} of all AMIP-p4K models. The global mean is slightly lower (-0.7%) compared to the AMIP models at 18.5%. As demonstrated in Figure 6c, most regions experience a decrease in PV_{pot}, particularly over the ice shields of Antarctica and Greenland, North America, and most regions of Asia and Australia. The strongest increases in PV_{pot} are seen over parts of Southeast Asia and Western Europe with a maximum of +1.7%.

4.1.2 Model differences

As illustrated in Figure 7, the AMIP simulations exhibit notable variations, with the ICON-ESM simulation (Figure 7a) achieving the lowest PV_{pot} with a global mean of 18.0%, exhibiting a near-universal negative deviation from the multi-model mean. Conversely, the MRI-ESM2-0 model (Figure 7f) exhibits the most pronounced positive deviations across all landmasses with a global mean of 20.3%.

The models MIROC6 (global mean: 19.1%, Figure 7e) and TaiESM1 (global mean: 19.0%, Figure 7g) show comparable patterns. Positive differences are seen over Northern Russia and North America, while negative differences are distributed over Africa and South America, indicating higher differences between the Northern and Southern hemispheres. The BCC-CSM2-MR model (global mean: 19.1%, Figure 7b) and the MPI-ESM1-2-LR model (global mean: 19.3%, Figure 7h) exhibit contrasting results, again demonstrating the variability in model outputs. The CESM2 (Figure 7c) and the IPSL-CM6A-LR model (Figure 7d) show the least deviations from the multi-model mean. Table 3a shows the mean values for every model and region. The analysis indicates that the PV_{pot} calculated with the ICON-ESM simulation is the lowest globally (18.0%) and over the area of Europe (13.6%), but not over Austria (13.8%) and Vienna (13.7%). The MRI-ESM2-0 model reached the highest results over all regions.

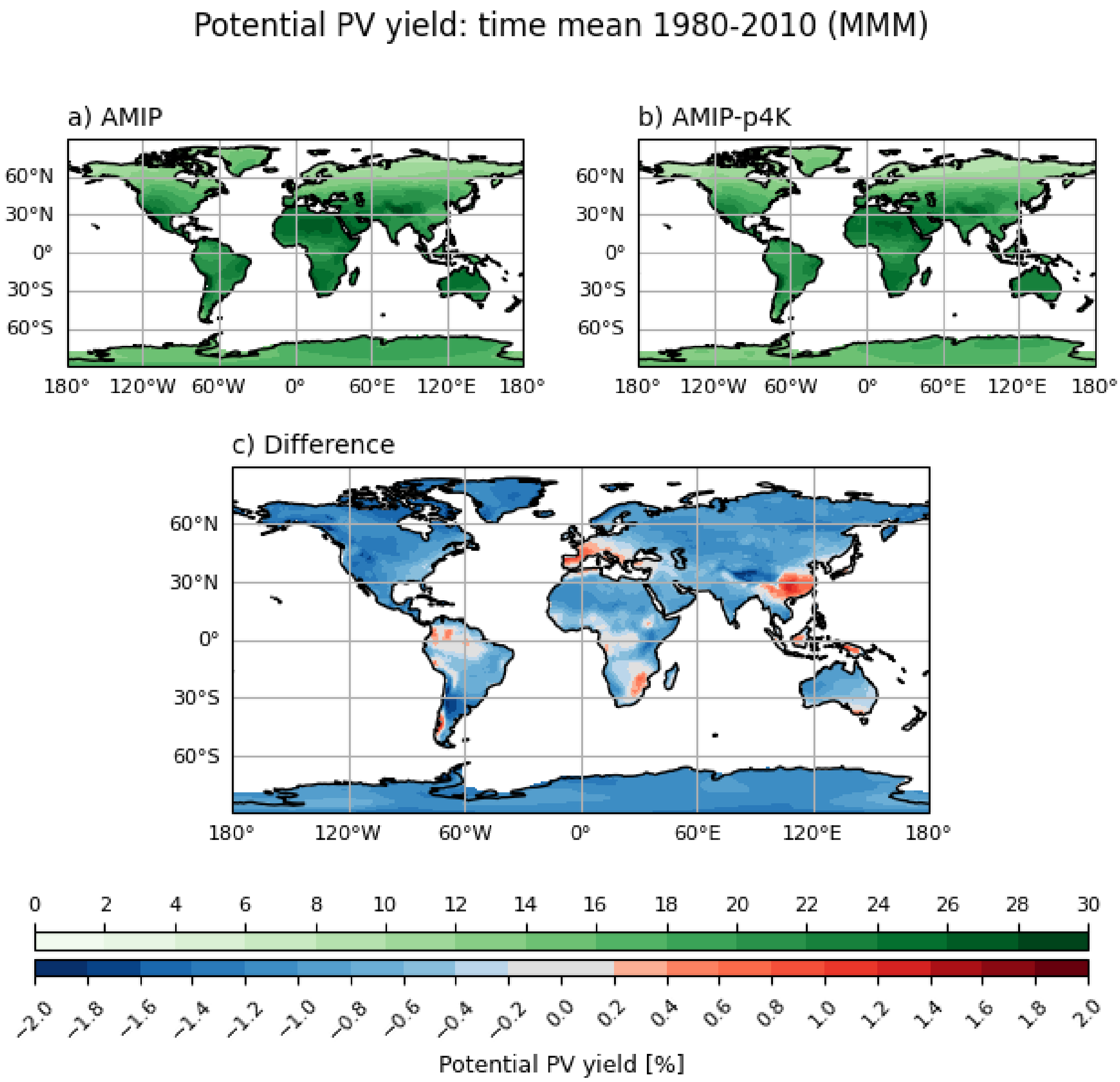

Figure 6: Time (1980-2010) and multi-model mean (MMM) of the CMIP6 models and the ICON simulation for (a) an AMIP and (b) an AMIP-p4K and (c) the absolute difference between AMIP and AMIP-p4K. The colorbars show PV_{pot} in %, where the first colorbar shows values for figures a and b, and the second shows values for figure c.

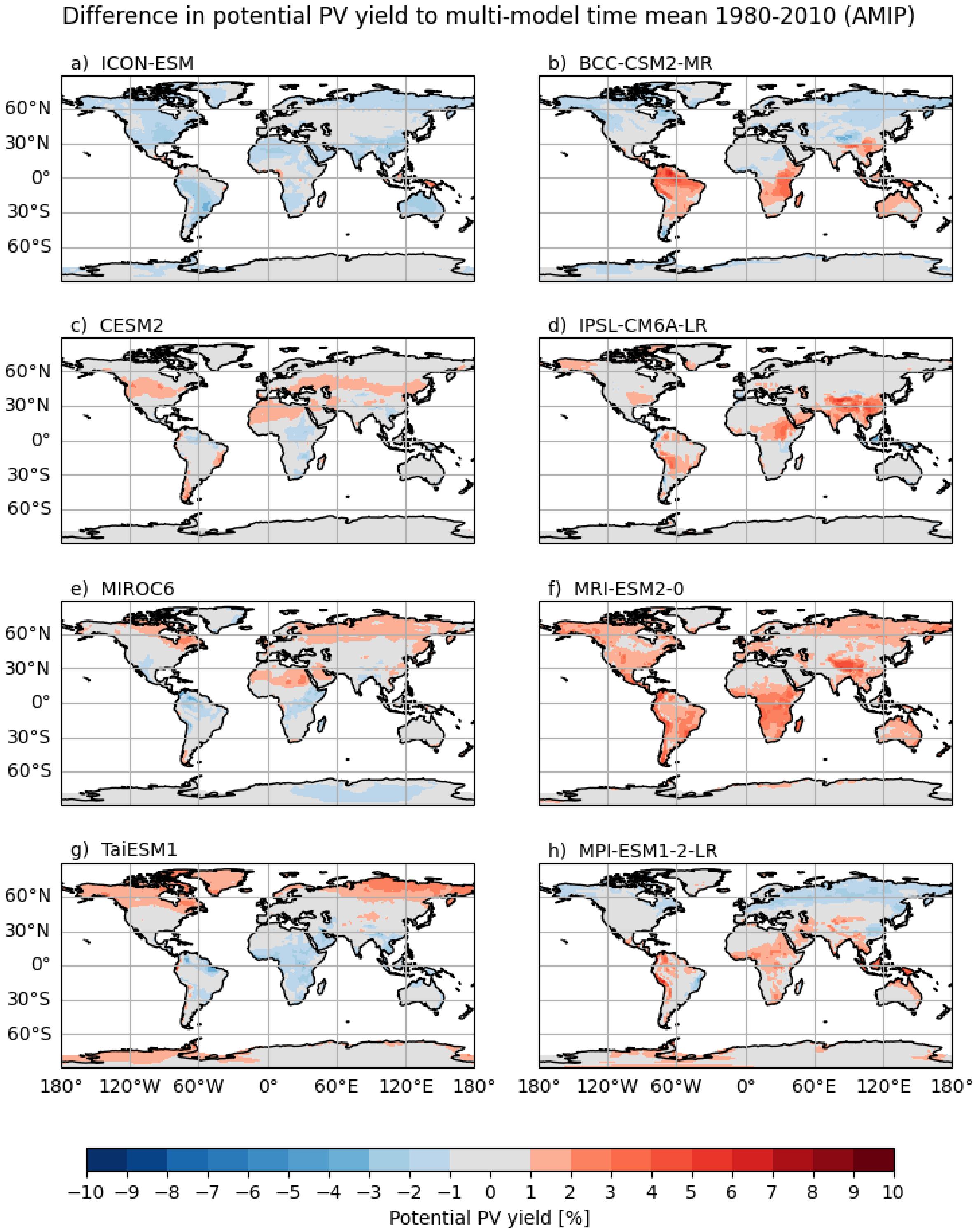

Figure 7: Differences to multi-model mean PV_{pot} (temporal mean 1980-2010).

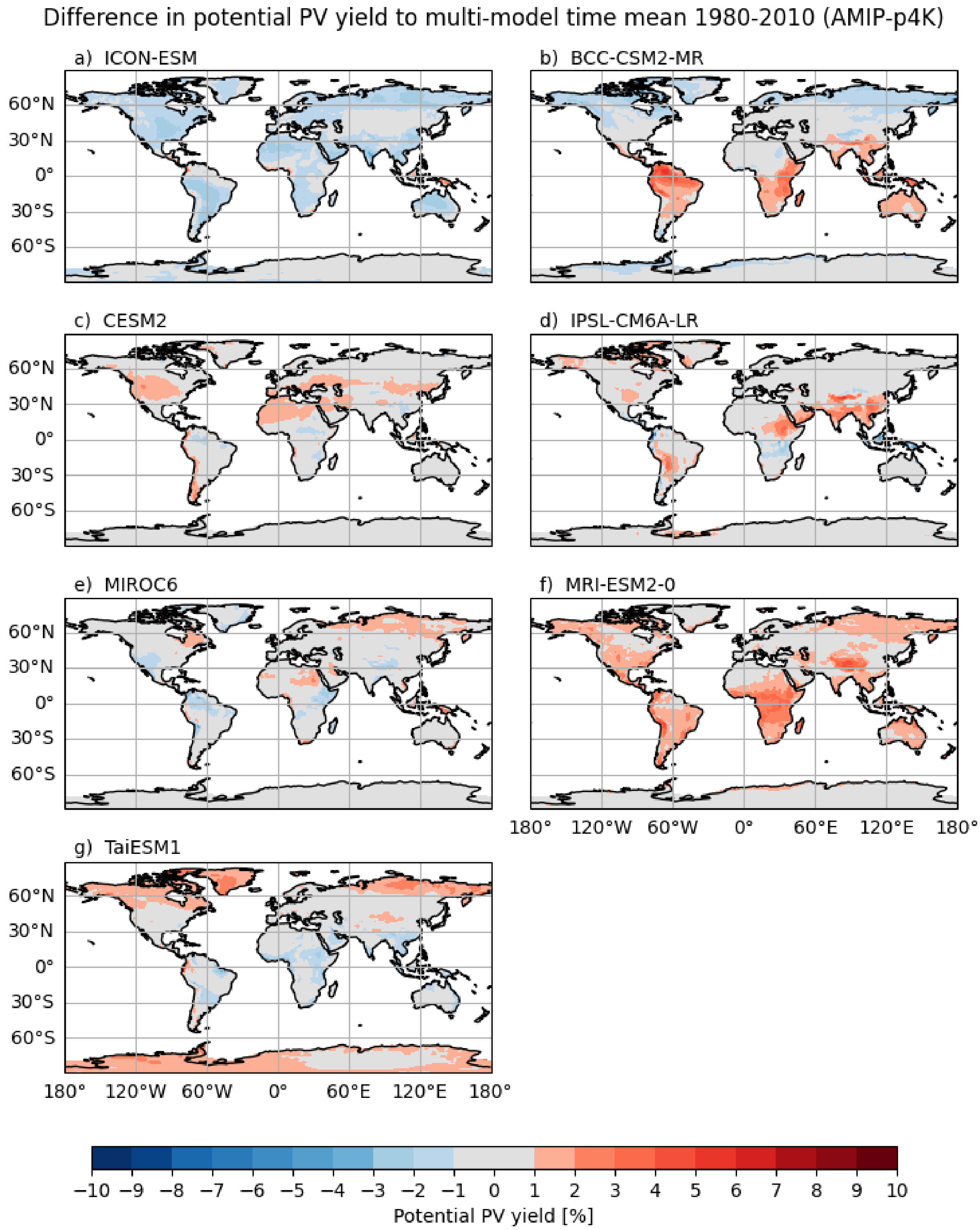

Figure 8: Differences to multi-model mean PV_{pot} (temporal mean 1980-2010).

Table 3: Temporal and spatial mean PV_{pot} (%) globally, over Europe, Austria and Vienna for the period 1980-2010 for all CMIP6 and ICON-ESM models for a) the AMIP models and b) the AMIP-p4K models.

(a)

	ICON-ESM	**BCC-CSM2-MR**	**CESM2**	**IPSL-CM6A-LR**	**MIROC6**	**MRI-ESM2-0**	**TaiESM1**	**MPI-ESM1-2-LR**	**MMM**	**Spread**
Global	18.0	19.1	19.3	19.5	19.1	20.3	19.0	19.3	19.2	2.3
Europe	13.6	13.6	14.9	14.4	14.9	15.0	14.8	13.5	14.3	1.4
Austria	13.8	13.3	14.4	15.0	14.4	15.4	14.8	13.9	14.4	2.1
Vienna	13.7	13.6	14.6	14.8	14.4	15.2	15.4	14.5	14.5	1.8

(b)

	ICON-ESM	**BCC-CSM2-MR**	**CESM2**	**IPSL-CM6A-LR**	**MIROC6**	**MRI-ESM2-0**	**TaiESM1**	**MMM**	**Spread**
Global	17.2	18.6	18.7	18.7	18.4	19.6	18.5	18.5	2.4
Europe	12.9	13.4	14.8	14.0	14.4	14.6	14.7	14.1	1.8
Austria	13.4	14.1	14.7	14.4	14.8	15.4	15.4	14.6	2.1
Vienna	13.4	14.3	15.0	14.5	14.7	15.4	15.9	14.7	2.5

There was a high degree of similarity between the spatial differences of the AMIP-p4K simulations and those of the AMIP simulations, as seen in Figure 8. The ICON-ESM simulation (Figure 8a) is again achieving the lowest PV_{pot} with a global mean of 17.2% and the MRI-ESM2-0 model (Figure 8f) the highest deviations with a global mean of 19.6% and similar located negative deviation from the multi-model mean. The models CESM2 (global mean: 18.7%, Figure 8c), MIROC6 (global mean: 18.4%, Figure 8e) and TaiESM1 (global mean: 18.5%, Figure 8g) demonstrate comparable PV_{pot} patterns to the AMIP simulation setup with positive differences over Northern Russia and North America and negative differences over Africa and South America. The BCC-CSM2-MR model (global mean: 18.6%, Figure 8b) shows similar differences to the AMIP setup as well. An exception is the IPSL-CM6A-LR model (global mean: 18.7%, Figure 8d) as it shows the least deviations from the multi-model mean but the existing deviations grew in magnitude, as well as showing negative changes over parts of Africa. As seen in Table 3b, the ICON-ESM model provides the lowest PV_{pot} globally (17.2%) and over Europe (12.9%). Contrary to the AMIP simulation, the ICON-ESM model also reaches the lowest results for regions of Austria and Vienna (both 13.4%).

As demonstrated in Figure 9, an analysis of the global mean PV_{pot} per average day of the year reveals seasonal variations in all models, with slightly higher values during the Northern hemisphere summer months, peaking around June and July. The higher amount of land masses in the Northern hemisphere is the likely cause of this phenomenon.

For time series over all regions, see appendix, Figure 27.

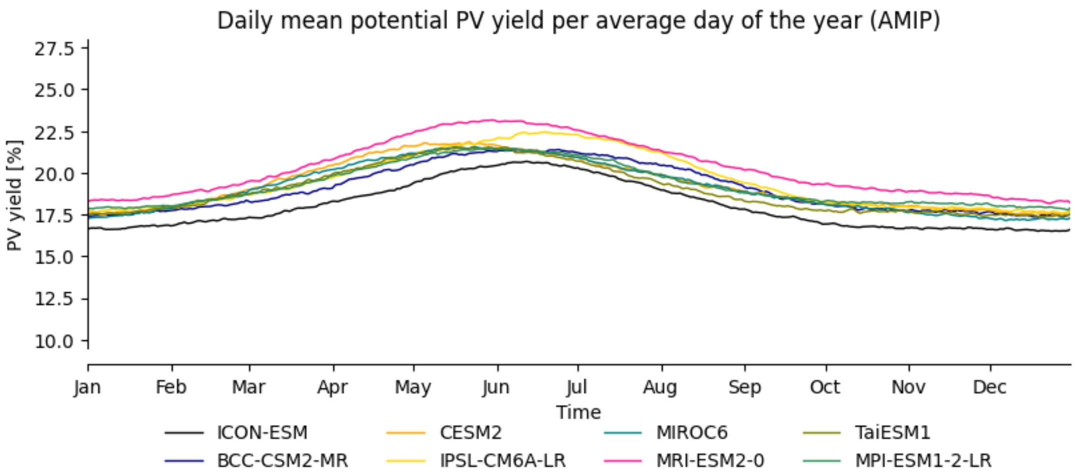

Figure 9: Global-mean daily-mean PV_{pot} in the AMIP simulations as a function of the day of the year (1980-2010).

As shown in Figure 10, this pattern is replicated in the AMIP-p4K simulations, with the peak time of the year remaining consistent across all simulations. Over the whole year, all models' PV_{pot} was lower than in the AMIP simulations.

Figure 11 shows the time and model-mean difference between the AMIP and AMIP-p4K simulations during the period JJA. As anticipated, the deviations across the northern hemisphere are the most significant during the summer months. Notably, the changes across the ice shields in Greenland are particularly pronounced.

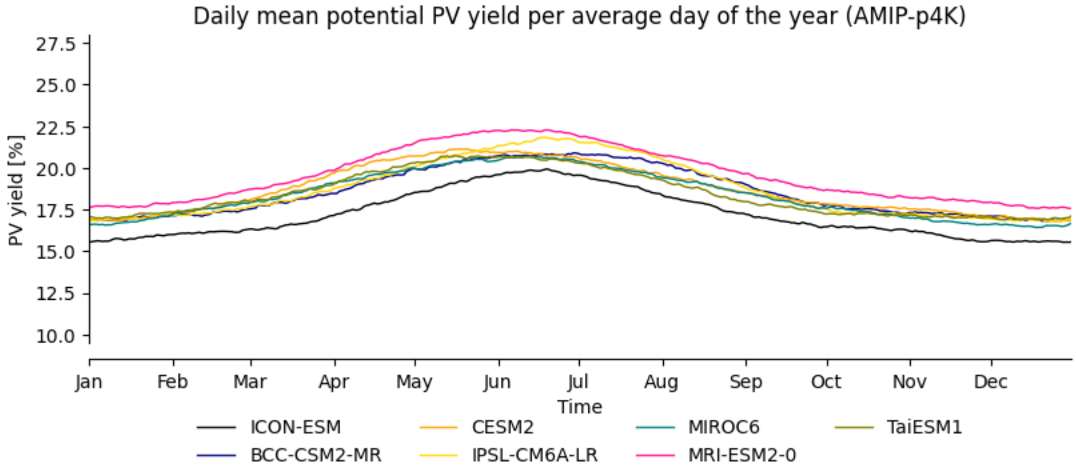

Figure 10: Global-mean daily-mean PV_{pot} in the AMIP-p4K simulations as a function of the day of the year (1980-2010).

In contrast, positive changes are evident across most of Europe, where high levels of irradiation can be seen during summer months. Negative changes are found in North America and Africa. These findings hint at the adverse effects of high temperatures on photovoltaic production. The highest positive changes can be found over the Himalayan mountain range. As illustrated in Figure 12, there are again strong negative changes over the ice shields during the season DJF. The most pronounced changes can be found over the southern Andes. Negative changes can be found over areas with high temperatures during DJF like Australia, Africa and South America.

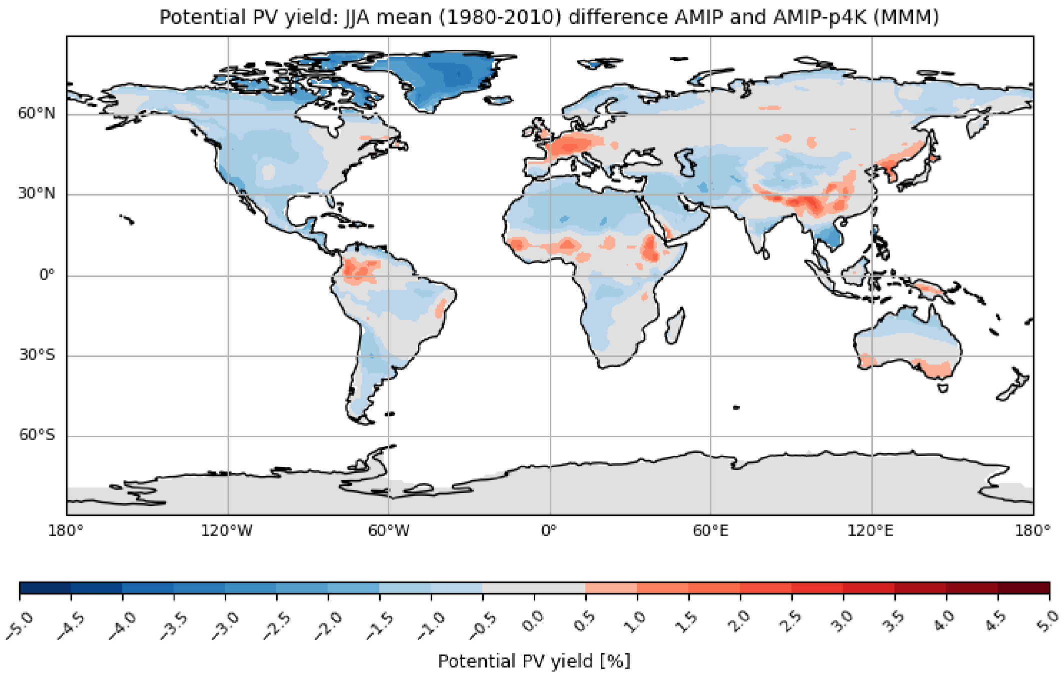

Figure 11: Time (1980-2010) and multi-model mean (MMM) PV_{pot} difference of the MMM AMIP and MMM AMIP-p4K simulations during JJA

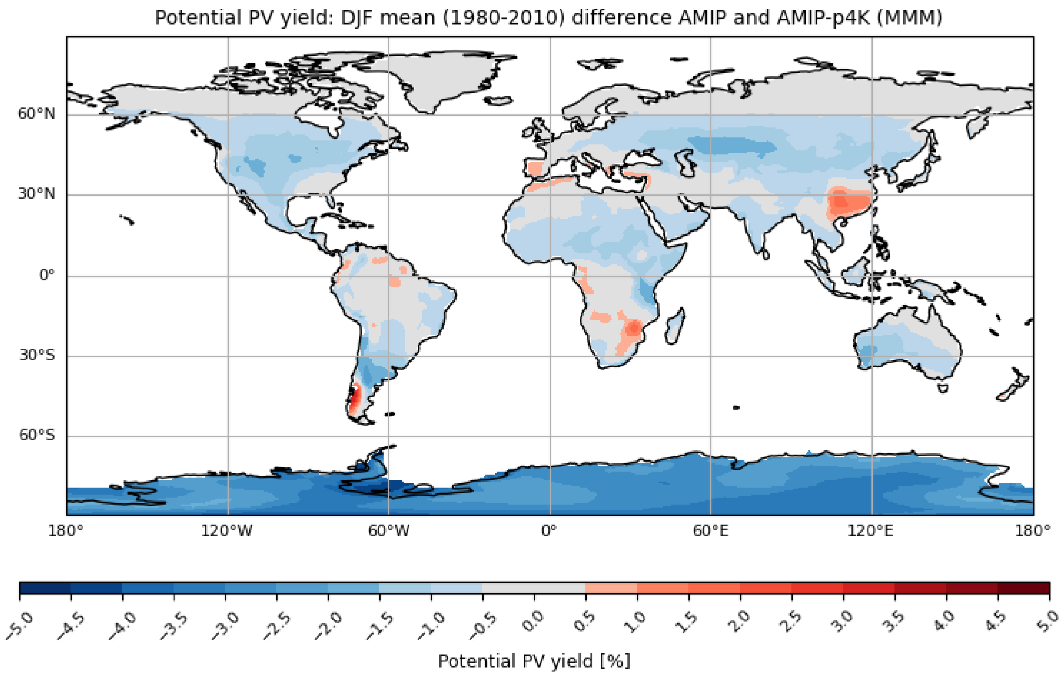

Figure 12: Time (1980-2010) and multi-model mean (MMM) PV_{pot} difference of the MMM AMIP and MMM AMIP-p4K simulations during DJF

4.2 Comparison of daily mean and daily maximum PV_{pot}

Excess photovoltaic power production has the potential to cause problems for consumers and utility companies. Overproduction leads to shift in the grid frequency, which in turn can lead to a grid overload. To prevent damages to the grid, the excess power is often wasted to ensure the integrity of equipment, inverters and even electrical grid infrastructures (Gecko Solar Energy, 2024; Hannam, 2024).

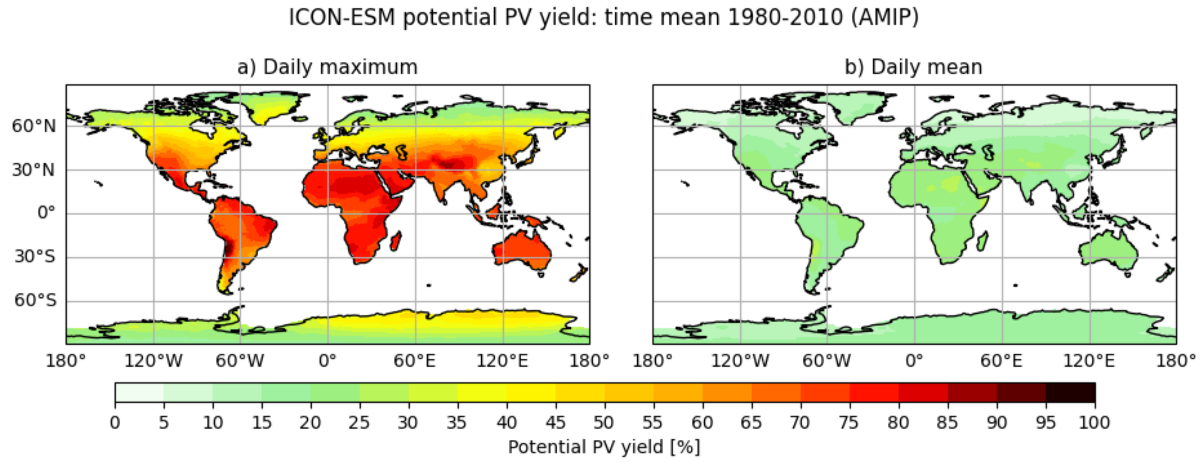

Figure 13: ICON-ESM AMIP simulation temporal mean (1980-2010) PV_{pot} calculated with a) daily maximum and b) daily mean input data.

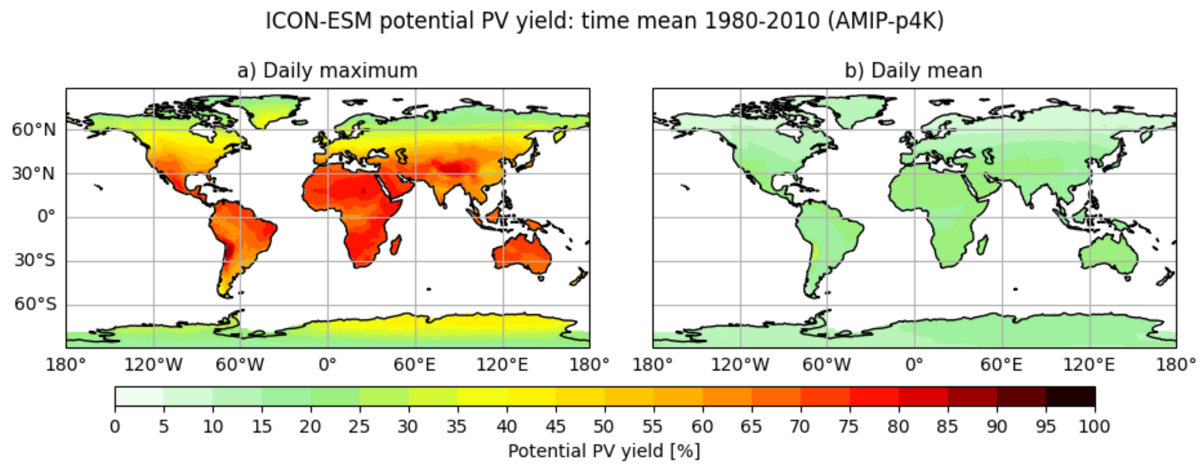

Figure 14: ICON-ESM AMIP-p4K simulation temporal mean (1980-2010) PV_{pot} calculated with a) daily maximum and b) daily mean input data.

Figures 13 and 14 show a comparison of the time-averaged PV_{pot} calculated from daily maximum and daily mean input data. The daily maximum PV_{pot} values are shown in figures 13a and 14a, for the AMIP and the AMIP-p4K simulation respectively. As anticipated, the highest PV_{pot} is seen in the tropics, where year-round high radiation levels are prevalent. Conversely, the PV_{pot} exhibits a decline towards the poles.

The maximum PV_{pot} was determined to be 95.3% for the AMIP and 88.6 % for the AMIP-p4K simulation. The regions with the highest PV_{pot} are the Himalayas, Central America and northern Africa. The global mean daily maximum PV_{pot} for the AMIP simulation was determined to be 46.7% while the result for the the AMIP-p4K reduced to 44.1%.

As demonstrated in Figure 13b and Figure 14b, the PV_{pot} calculated with daily mean input data was found to be considerably lower compared to the daily maximum PV_{pot} with a decline of -30.2% for the AMIP and -28.6% for the AMIP-p4K simulation.

In tune with previous studies, the global mean PV_{pot} calculated with daily maximum input values from the AMIP-p4K simulation decreased compared to the AMIP simulation (-2.6%).

Figure 15 shows the mean and maximum PV_{pot} per day of the year, averaged globally, over Europe, over Austria and over Vienna. As expected, there are greater daily fluctuations in the smaller regions. The maximum PV_{pot} reaches a maximum during the summer months in Europe (70.5%), Austria (76.1%) and Vienna (77.1%), while the global mean shows only small seasonal variations (seasonal difference: 11.8%). During the winter months in Austria and Vienna the mean PV_{pot} reaches a minimum of 11.8% and 10.4% respectively, a difference of around 60%. As can be seen in Figure 16, the maximum PV_{pot} over the northern hemisphere summer months decreases globally (-3.0%), over Europe (-3.6%), over Austria (-1.8%) and over Vienna (-0.9%). On the other hand, the winter minimum over Vienna increases to a PV_{pot} of 12.1% and the minima over Austria and Europe increase slightly compared to the AMIP simulation.

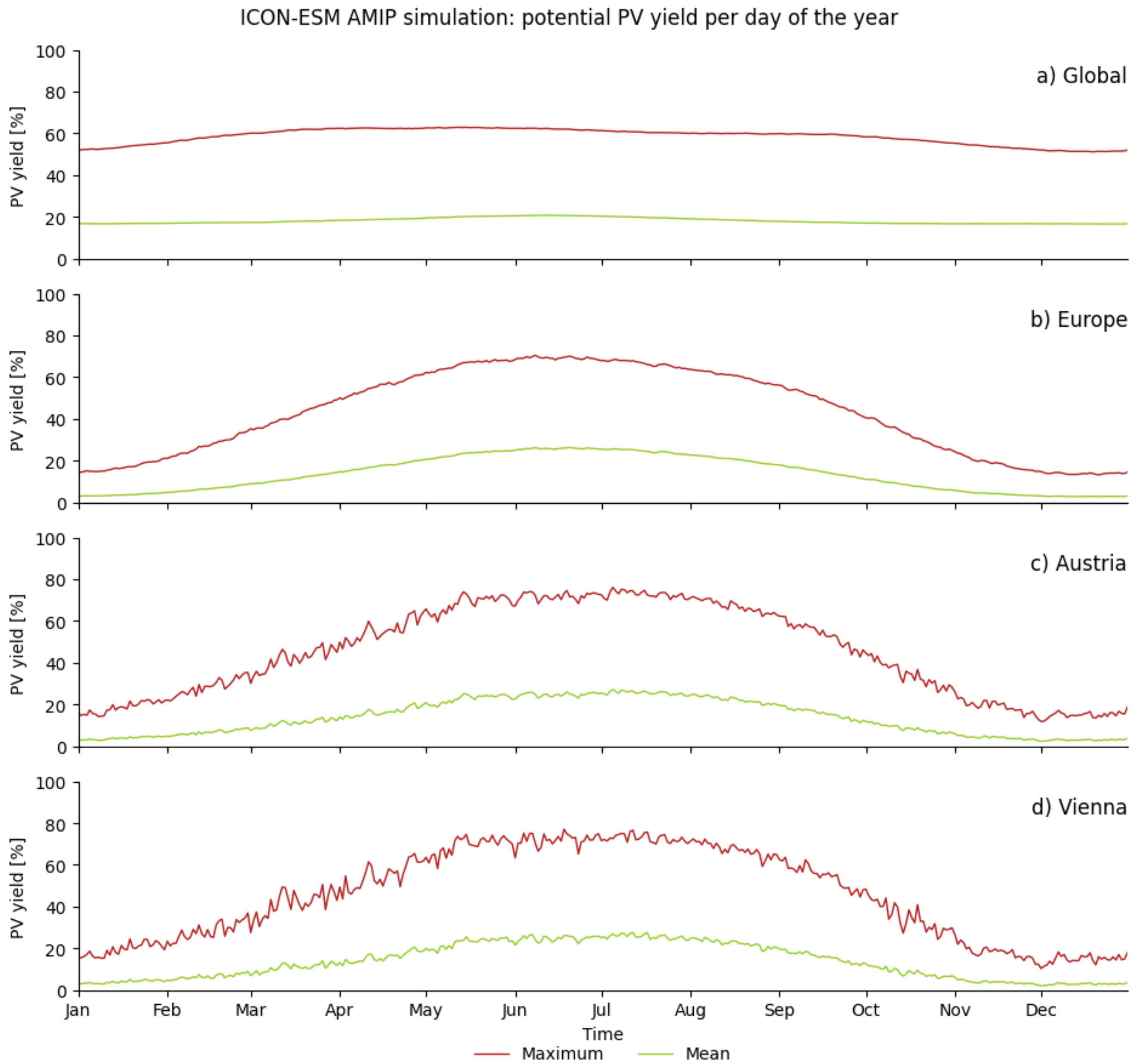

Figure 15: PV_{pot} calculated with daily mean and daily maximum output of the ICON-ESM AMIP simulation as a function of the day of the year (1980-2010) averaged globally, over Europe, over Austria and over Vienna.

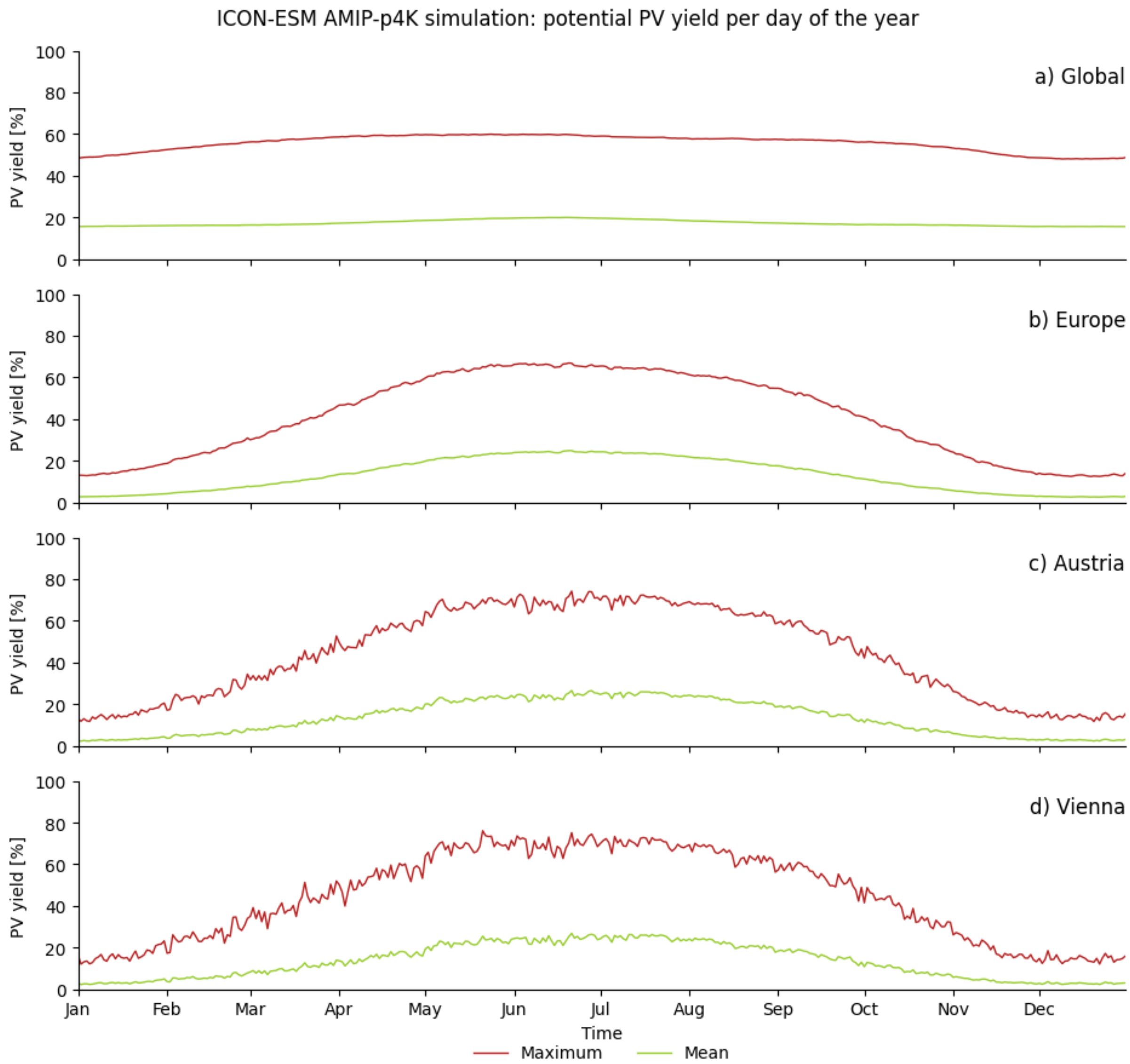

Figure 16: PV_{pot} calculated with daily mean and daily maximum output of the ICON-ESM AMIP-p4K simulation as a function of the day of the year (1980-2010) averaged globally, over Europe, over Austria and over Vienna.

4.3 Comparison of errors in PV_{pot} calculation due to time-averaging

For this analysis, I averaged the input data with a time resolution of 15-minute to seven additional time periods and calculated the PV_{pot} eight times. Given that the ICON-ESM simulations provide an output at 15-minute intervals and previous studies utilised daily mean data, I chose the time resolutions to be 15 minutes, 30 minutes, 1 hour, 3 hours, 4 hours, 6 hours, 12 hours and 24 hours. I selected the additional time periods to achieve a range of time resolutions and because these are under the most commonly available resolutions of climate data. Thereafter, I conducted a comprehensive analysis of the results on a monthly basis, considering four distinct regions (globally, Europe, Austria and Vienna) and each averaging period.

4.3.1 Global mean PV_{pot} per time resolution of the input data

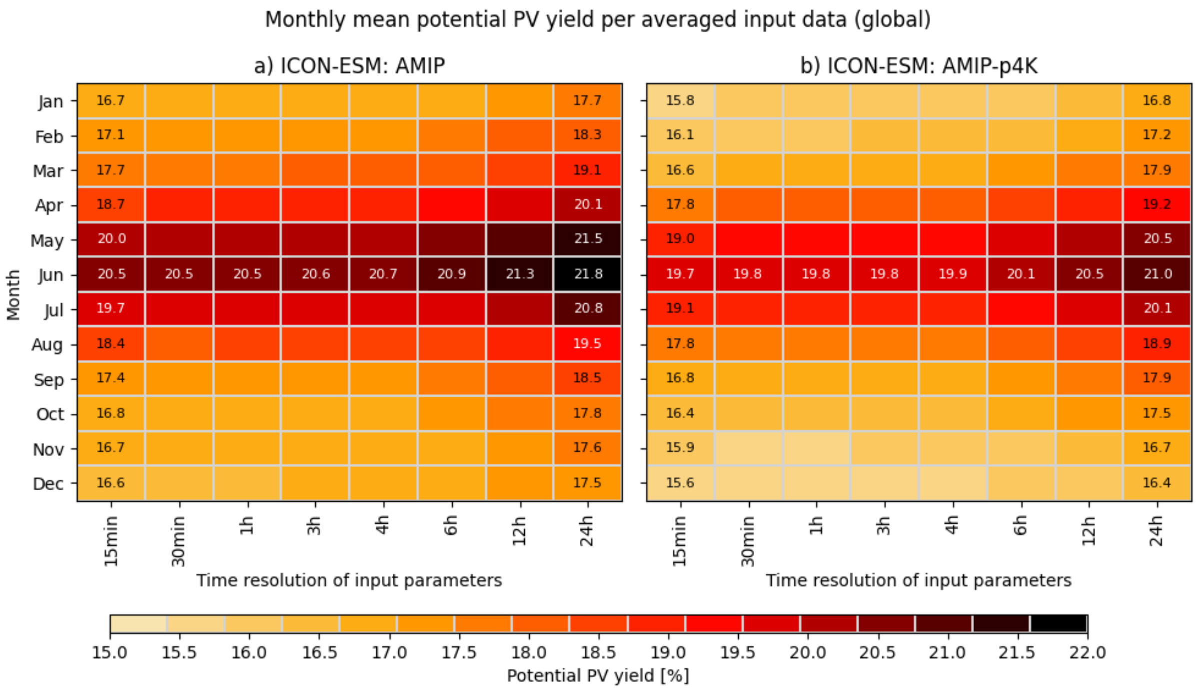

Figure 17: Monthly and global mean PV_{pot} from ICON-ESM a) AMIP simulation and b) AMIP-p4K simulation data with different time resolutions. The x-axes indicate the averaging period and the y-axes the month of the year. The colorbar shows PV_{pot} in %.

The global monthly mean PV_{pot} is presented in Figure 17a for the AMIP simulation and in Figure 17b for the AMIP-p4K simulation. The differences between the time resolutions are evident throughout the year, with the most pronounced differences occurring in June and the smallest in December. This phenomenon is directly associated with a greater proportion of landmasses in the northern hemisphere compared to the southern hemisphere. In December, the PV_{pot} was overestimated by +0.9% (relative: +5.4%) for the AMIP simulation and +0.8% (relative: +5.1%) for the AMIP-p4K simulation.

Table 4: Deviations of PV_{pot} yield in %, calculated with averaged input data, in comparison to the native time resolution (15 minutes) of ICON-ESM a) AMIP and b) AMIP-p4K simulation during the month with the PV_{pot}.

(a)

	Results (15 min.)	**30 minutes**	**1 hour**	**3 hours**	**4 hours**	**6 hours**	**12 hours**	**24 hours**
Global (June)	20.5	0.0	0.0	+0.1	+0.2	+0.4	+0.8	+1.3
Europe (June)	25.6	0.0	+0.1	+0.1	+0.2	+0.4	+1.4	+1.5
Austria (July)	25.6	−0.1	−0.1	0.0	+0.1	+0.3	+1.5	+1.5
Vienna (July)	25.7	−0.9	−0.9	−0.8	−0.8	−0.6	+0.6	+1.5

(b)

	Results (15 min.)	**30 minutes**	**1 hour**	**3 hours**	**4 hours**	**6 hours**	**12 hours**	**24 hours**
Global (June)	19.7	+0.1	+0.1	+0.1	+0.2	+0.4	+0.8	+1.3
Europe (June)	24.0	+0.1	+0.1	+0.2	+0.2	+0.4	+1.4	+1.4
Austria (July)	24.8	−0.1	−0.1	0.0	+0.1	+0.3	+1.5	+1.5
Vienna (July)	24.9	−0.1	−0.1	0.0	0.0	+0.2	+1.4	+1.4

As the averaging period extends, the monthly average PV_{pot} is increasingly overestimated. Table 4 shows that the most significant deviation occurs after the application of the 6-hour, 12-hour and 24-hour averaging periods. For the month with the highest PV_{pot} (June) in the AMIP simulation, there are no significant deviations for the 30-minutes and 1-hour period and only an error of +0.1% and +0.2% for the 3-hour and 4-hour period. After averaging the input data to a time resolution of six hours, the error doubles to +0.4% and again doubles to +0.8% after applying the 12-hour averaging. After the 24-hour averaging the difference is +1.3%, which equates to a relative difference of +6.3%. The global model spread for the AMIP simulations in Section 4.1 is 2.3%, which is higher than the error because of time-averaging. The averaged AMIP-p4K simulation shows a similar pattern to the AMIP simulation. The errors for the 30-minutes, 1-hour and 3-hour averaging period are small with +0.1%. For the other time periods, an error of +0.2% was found for the 4-hour period, +0.4% for the 6-hour period and +0.8% for the 12-hour period. For the 24-hour period, the error was again +1.3% which equates to a relative difference of +5.1%. The global model spread for the AMIP-p4K simulations in Section 4.1 is 2.4%, which is again higher than the error because of time averaging.

4.3.2 Mean PV_{pot} over Europe per time resolution of the input data

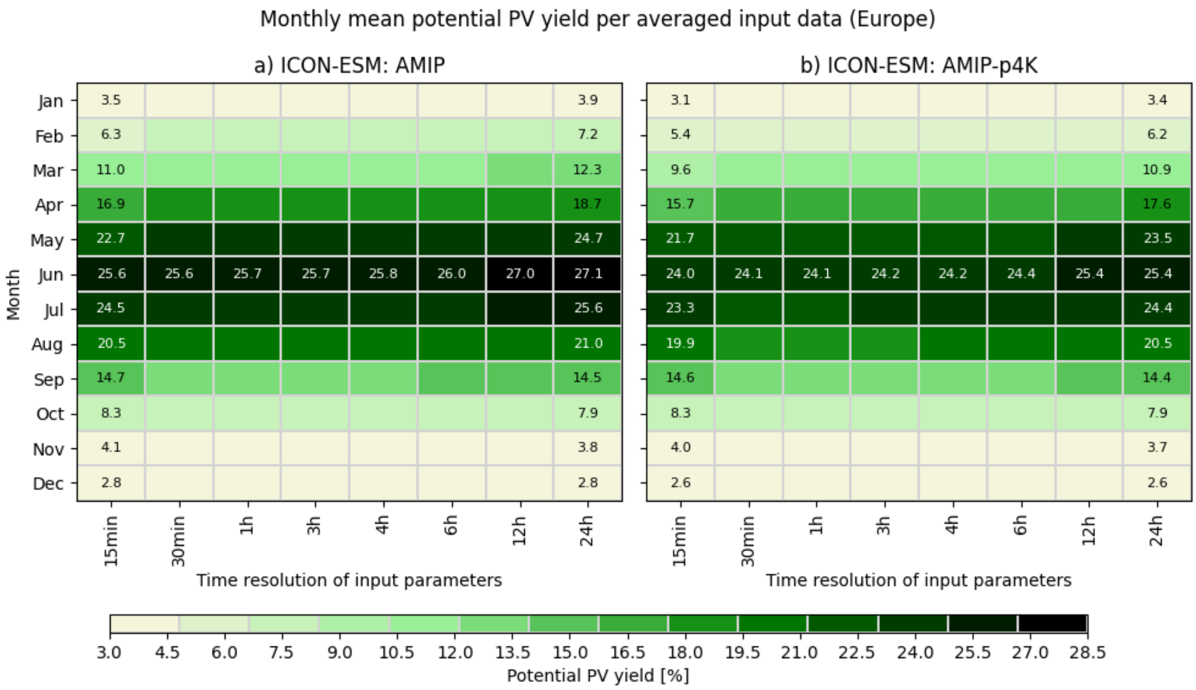

Figure 18: Monthly mean PV_{pot} over Europe from ICON-ESM a) AMIP simulation and b) AMIP-p4K simulation data with different time resolutions. The x-axes indicate the averaging period and the y-axes the month of the year. The colorbar shows PV_{pot} in %.

Figure 18 illustrates the monthly mean PV_{pot} for Europe. The data has been averaged over the area of Europe for the AMIP simulation in Figure 18a and for the AMIP-p4K simulation in Figure 18b. In comparison to the global monthly mean PV_{pot} depicted in Figure 17, there are strong seasonal variations in Europe. The period from May to August is characterised by higher PV_{pot} in comparison to the global average for all considered periods, while the months of September to April are associated with a lower PV_{pot}.

The comparison of the global analysis and the analysis over Europe suggests that larger overestimations occur due to time averaging during the European summer months in comparison to the same period on a global scale. This indicates a correlation between warmer seasons and overestimation of the PV_{pot} because of time averaged data.

In the AMIP simulation during the month of June, the deviation from the 15-minutes resolution is comparable to the errors on a global scale, as seen in Table 4. For the 1-hour and 3-hour periods the error is +0.1%, for the 4-hour period +0.2% and for the 6-hour period +0.4%. Contrary to the global dataset, the error for the 12-hour period and the 24-hour period amounts to similar values at +1.4% and +1.5%, which corresponds to a relative increase of +5.5% and +5.9%. In December, the overestimation is negligible, with a value of zero percent. The model spread for the AMIP simulations over Europe is 1.4% and therefore very similar to the error due to time-averaging.

For the AMIP-p4K simulation, the errors are again very similar to the AMIP simulation. The error for the 24-hour period is +1.4% (relative: +5.8%), which is lower than in the AMIP simulation. In December, the overestimation again is negligible. The AMIP-p4K model spread over Europe is 1.8%, which is slightly higher than the error due to time-averaging. The 12-hour and 24-hour averaging results in a similar error.

4.3.3 Mean PV_{pot} over Austria and Vienna per time resolution of the input data

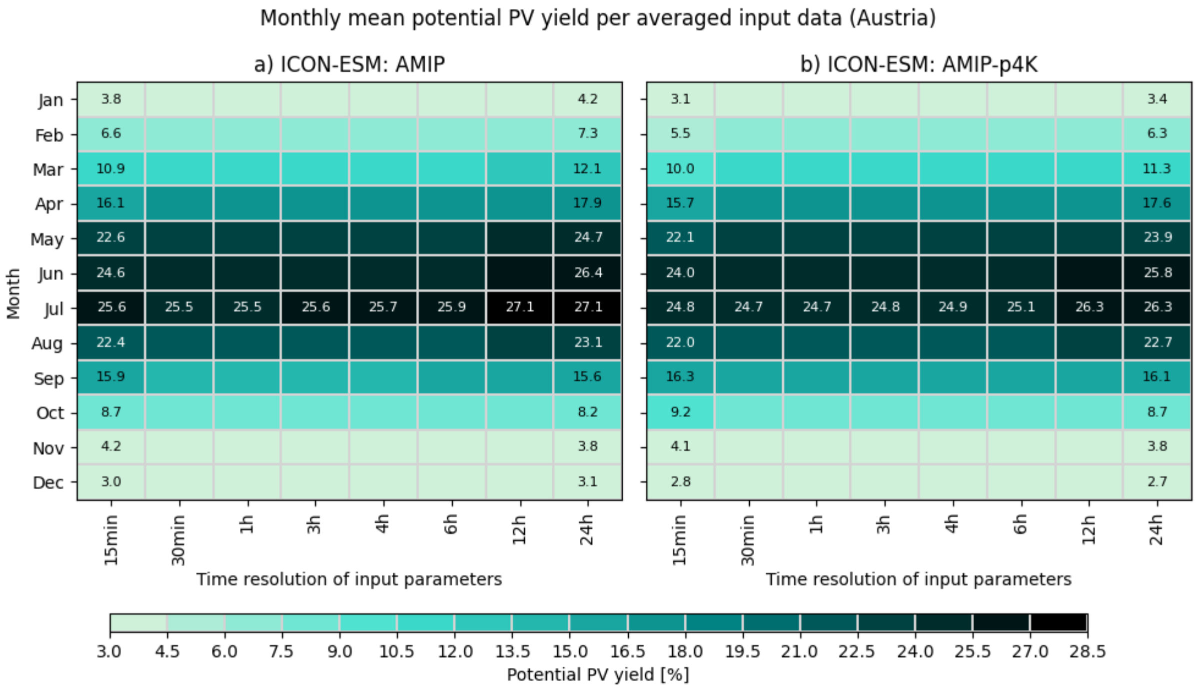

Figure 19: Monthly mean PV_{pot} over Austria from ICON-ESM a) AMIP simulation and b) AMIP-p4K simulation data with different time resolutions. The x-axes indicate the averaging period and the y-axes the month of the year. The colorbar shows PV_{pot} in %.

The monthly average PV_{pot} for Austria is shown in Figure 19 and the monthly average PV_{pot} for Vienna is shown in Figure 20. It is evident that the PV_{pot} for both Austria and Vienna show a notable similarity, with the highest values found in July and the lowest in December. The seasonality over Austria and Vienna is similar to the whole European continent. In December, the PV_{pot} reaches its minimum in Austria and Vienna. The discrepancy between the AMIP and the AMIP-p4K simulation diminishes throughout the colder months of the year.

For the dataset over Austria the AMIP and the AMIP-p4K simulation are equal to one percentage point. Table 4 shows that for the month of July for the 30-minutes and 1-hour periods, the error reaches negative values at -0.1%. For the 3-hour period the error is negligible. For the 4-hour period the error is +0.1%, for the 6-hour period +0.3% and for the 12 and 24-hour periods 1.5%. This shows a similar pattern to the European data, that also showed similar values for the 12 and 24-hour periods. The model spreads for the AMIP and the AMIP-p4K simulations in Section 4.1 is 2.1% for Austria.

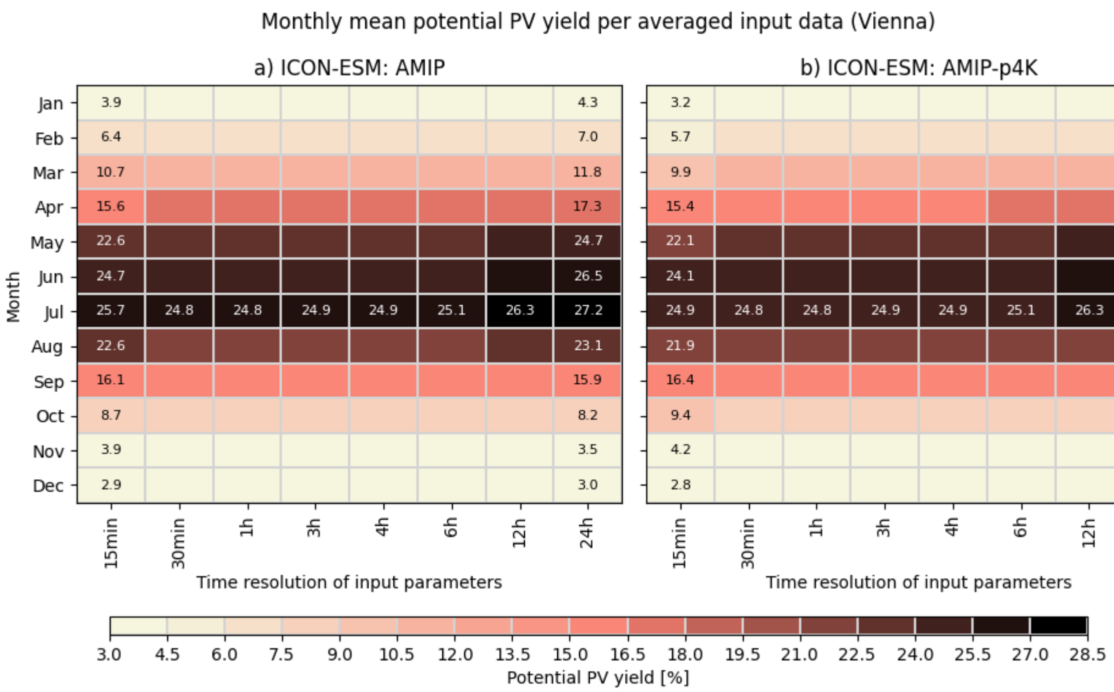

Figure 20: Monthly mean PV_{pot} over Vienna calculated with input data from the ICON-ESM a) AMIP simulation and b) AMIP-p4K simulation with different time resolutions. The x-axes indicate the averaging period and the y-axes the month of the year. The colorbar shows PV_{pot} in %.

The data over Vienna shows dissimilar patterns. For the AMIP simulation, all periods shorter than 12 hours show negative deviation compared to the 15-minutes dataset. The error for the 30-minutes and 1-hour periods is -0.9%, for the 3-hour and 4-hour -0.8% and for the 6-hour period -0.6%. The error for the 12-hour and 24-hour periods on the other hand is positive, with +0.6% and +1.5% respectively.

For the AMIP-p4K simulation, the errors for the 30-minutes and 1-hour periods are again negative at -0.1% and negotiable for the 3-hour and 4-hour period. For the 6-hour period the error is +0.2% and +1.4% for the 12-hour and 24-hour period.

The model spreads for the AMIP and AMIP-p4K simulations lies at 1.8% and 2.5% and is therefore slightly higher than the error due to time averaging.

5 Conclusion

My thesis studies the effects of time-averaging on the calculation of potential photovoltaic power yield. In addition to the research question, I found that globally, the PV_{pot} decreased in the AMIP-p4K simulations compared to the AMIP simulations.

My research question formulated for this study is as follows:

What is the error in potential photovoltaic power yield (PV_{pot}) due to the use of time-averaged data?

Previous studies frequently employed daily mean or even monthly mean input data to analyse the future of photovoltaic power generation. In the initial phase of the present study, I examined seven CMIP6 AMIP models and one ICON-ESM AMIP simulation, as well as six CMIP6 AMIP-p4K models and one ICON-ESM AMIP-p4K simulation to determine the spread of PV_{pot} calculated with daily mean data. The analysis encompasses four distinct regions: Vienna, Austria, the whole European continent and all global landmasses.

Following the determination of the model spread, my analysis focuses on the ICON-ESM AMIP and AMIP-p4K simulations. I determined the daily maximum of the simulation output to calculate the daily maximum PV_{pot} and compared it to the daily mean PV_{pot}.

I averaged the input variables for the PV_{pot} calculation in the native time resolution of 15 minutes for seven additional time periods (30 minutes, 1 hour, 3 hours, 4 hours, 6 hours, 12 hours and 24 hours) and PV_{pot} was calculated for every month and every averaging period for the four regions from the above calculations. Finally, a comparison was made between the model spread and the deviations caused by the time-averaged input data.

The spread of PV_{pot} for all simulations and regions is between 1.4 and 2.3% with the lowest values found over the area of Europe. The errors due to time averaging rise with the length of the averaging period. During the months with the highest PV_{pot}, the error due to time averaging for the 30-minutes, 1 hour, 3 hours and 4 hours averaging period are small at a maximum of +0.2%. The area of Vienna poses an exception with a negative maximum error of -0.9% for the smallest periods. These findings underscore the necessity for a regional perspective when assessing the impact of time averaging. A significant increase in errors due to time-averaging is seen at a resolution of 6 hours, and this error increases at least twofold for every subsequent averaging period. For the 24-hour averaging period, the overestimation is between +1.3 to +1.5% for all regions. These values are in a similar range to the model spread determined for the daily mean data.

The comparison of the global and the regional analysis suggests larger overestimations during the summer months in comparison to the same period on a global scale. This indicates a correlation between warmer seasons and overestimation of the PV_{pot} because of time averaged data.

In summary, my findings demonstrate that the process of time averaging results in an overestimation of PV_{pot}. This relative overestimation was found to be approximately +6%. This overestimation remains consistent in simulations involving warmer temperatures (AMIP-p4K), though it increases in relative terms as the absolute PV_{pot} decreases.

Despite the ICON-ESM model consistently delivering the lowest absolute values for all regions compared to the CMIP6 models, it can be assumed that an overestimation caused by time averaging applies to all GCMs. In light of the findings of previous publications, which found that the results fell within the range of my calculated overestimation, it is evident that daily mean data sets are not suitable for PV power estimation.

Bibliography

Baur, S., Sanderson, B. M., Séférian, R., and Terray, L. 2024. Solar radiation modification challenges decarbonization with renewable solar energy. *Earth System Dynamics*, 15(2), pp 307–322. doi: 10.5194/esd-15-307-2024, URL: https://esd.copernicus.org/articles/15/307/2024/.

Chenni, R., Makhlouf, M., Kerbache, T., and Bouzid, A. 2007. A detailed modeling method for photovoltaic cells. *Energy*, 32, pp 1724–1730. doi: 10.1016/j.energy.2006.12.006.

Coupled Model Intercomparison Project IPO, 2024. CMIP Overview. URL: https://wcrp-cmip.org/cmip-overview/ (Accessed: 2024-09-16).

Crook, J. A., Jones, L. A., Forster, P. M., and Crook, R. 2011. Climate change impacts on future photovoltaic and concentrated solar power energy output. *Energy and Environmental Science*, 4, pp 3101–3109. doi: 10.1039/c1ee01495a.

E.ON Energie Deutschland GmbH, 2025. Nennleistung und installierte Leistung - einfach erklärt. URL: https://www.eon.de/de/gk/energiewissen/nennleistung-installierte-leistung.html (Accessed: 2025-01-04).

Feron, S., Cordero, R. R., Damiani, A., and Jackson, R. B. 2021. Climate change extremes and photovoltaic power output. *Nature Sustainability*, 4, pp 270–276. doi: 10.1038/s41893-020-00643-w.

Gates, W., Boyle, J., Covey, C., et al. 01 1999. An Overview of the Results of the Atmospheric Model Intercomparison Project (AMIP I). *Bulletin of the American Meteorological Society*, 81, pp 29–55. doi: 10.1175/1520-0477(1999)080<0029:AOOTRO>2.0.CO;2.

Gecko Solar Energy, 2024. Can Too Much Wattage from a Solar Panel Cause Problems? URL: https://geckosolarenergy.com/excess-solar-panel-wattage-problems/ (Accessed: 2025-02-14).

Hannam, P., 2024. Why are some Australian households about to be charged for generating too much solar power? URL: https://www.theguardian.com/australia-news/article/2024/may/19/why-are-some-australian-households-about-to-be-charged-for-generating-too-much-solar-power (Accessed: 2025-02-15).

Jerez, S., Tobin, I., Vautard, R., et al. 2015. The impact of climate change on photovoltaic power generation in Europe. *Nature Communications*, 6. doi: 10.1038/ncomms10014.

Jungclaus, J. H., Lorenz, S. J., Schmidt, H., et al. 2022. The ICON Earth System Model Version 1.0. *Journal of Advances in Modeling Earth Systems*, 14(4), pp e2021MS002813. doi: https://doi.org/10.1029/2021MS002813.

Panagea, I. S., Tsanis, I. K., Koutroulis, A. G., and Grillakis, M. G. 2014. Climate change impact on photovoltaic energy output: The case of Greece. *Advances in Meteorology*, 2014. doi: 10.1155/2014/264506.

Schulzweida, U., Oct. 2023. CDO User Guide. URL: `https://doi.org/10.5281/zenodo.10020800`.

Skoplaki, E. and Palyvos, J. A. 2009. On the temperature dependence of photovoltaic module electrical performance: A review of efficiency/power correlations. *Solar Energy*, 83, pp 614–624. doi: 10.1016/j.solener.2008.10.008.

Tamizhmani, G., Ji, L., Tang, Y., et al. 2003. Photovoltaic Module Thermal/Wind Performance: Long -Term Monitoring and Model Development For Energy Rating. Ncpv and solar program review meeting 2003, Arizona State University East, Photovoltaic Testing Laboratory.

Taylor, K. E., Balaji, V., Hankin, S., et al. 2012. CMIP5 Data Reference Syntax (DRS) and Controlled Vocabularies. online, URL: `https://pcmdi.llnl.gov/mips/cmip5/docs/cmip5_data_reference_syntax.pdf?id=3`.

Tonui, J. K. and Tripanagnostopoulos, Y. 2007. Improved PV/T solar collectors with heat extraction by forced or natural air circulation. *Renewable Energy*, 32, pp 623–637. doi: 10.1016/j.renene.2006.03.006.

Appendix

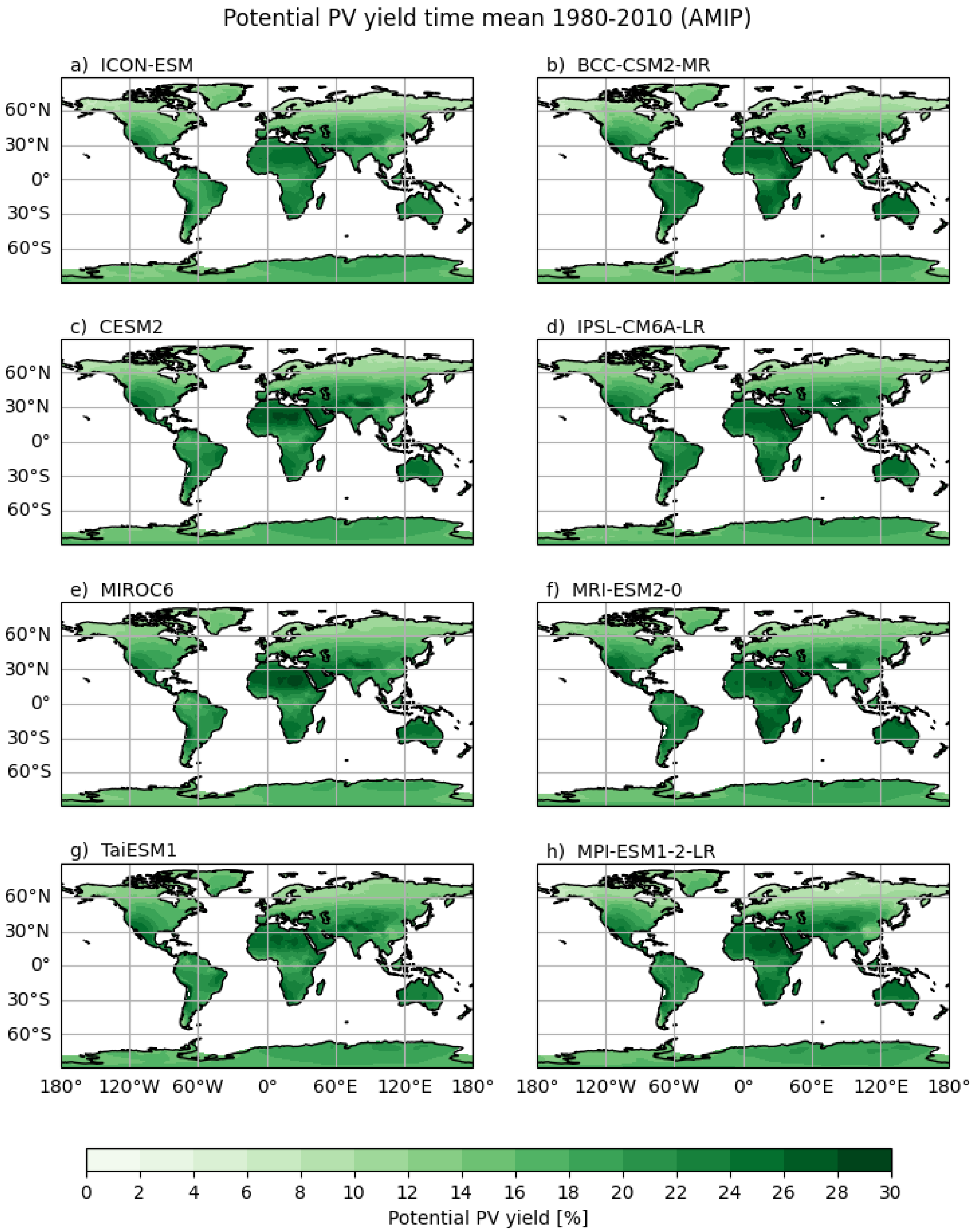

Figure 21: Time (1980-2010) mean potential PV yield for an ICON-ESM AMIP simulation and seven CMIP6 AMIP models.

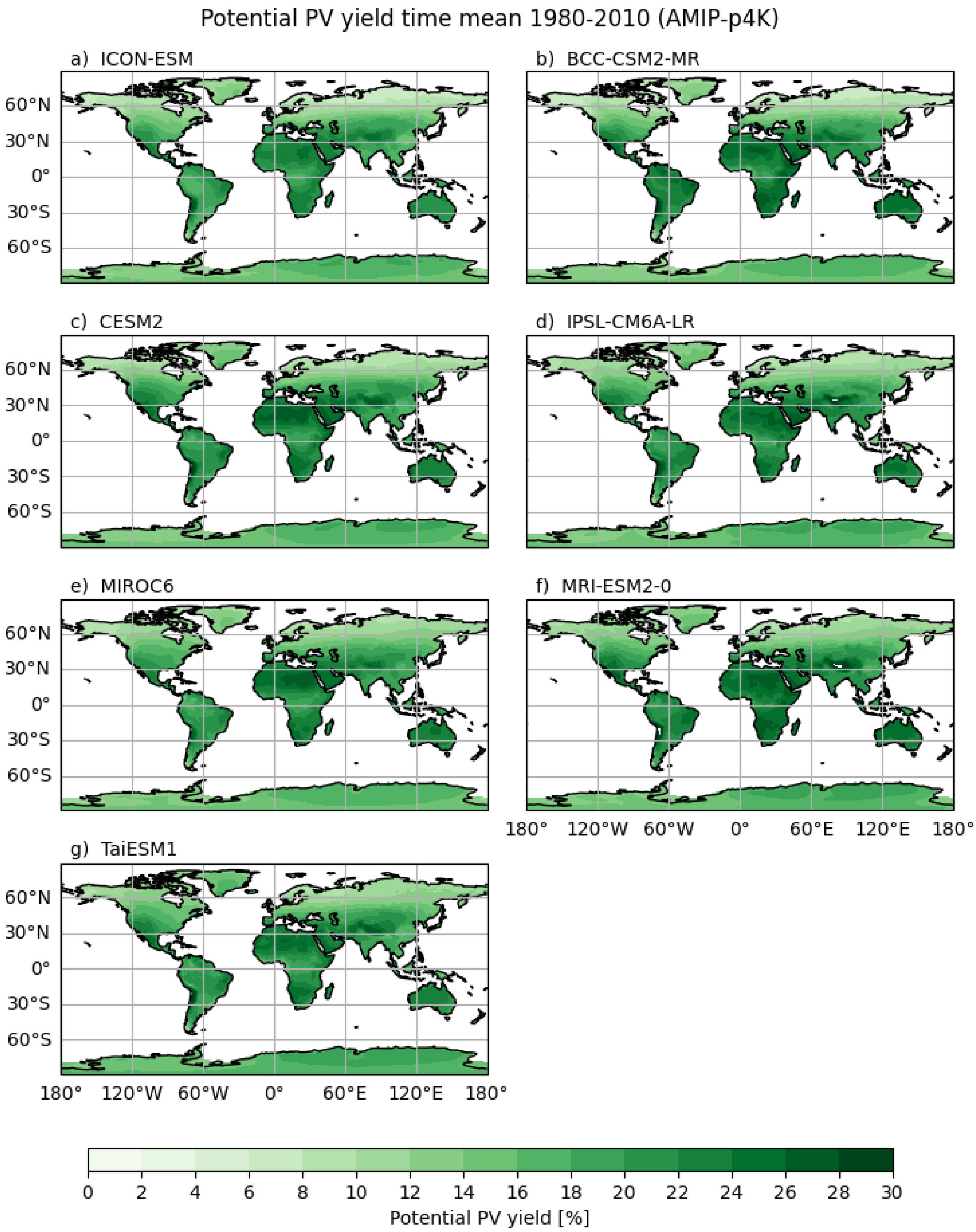

Figure 22: Time (1980-2010) mean potential PV yield for an ICON-ESM AMIP-p4K simulation and six CMIP6 AMIP-p4K models.

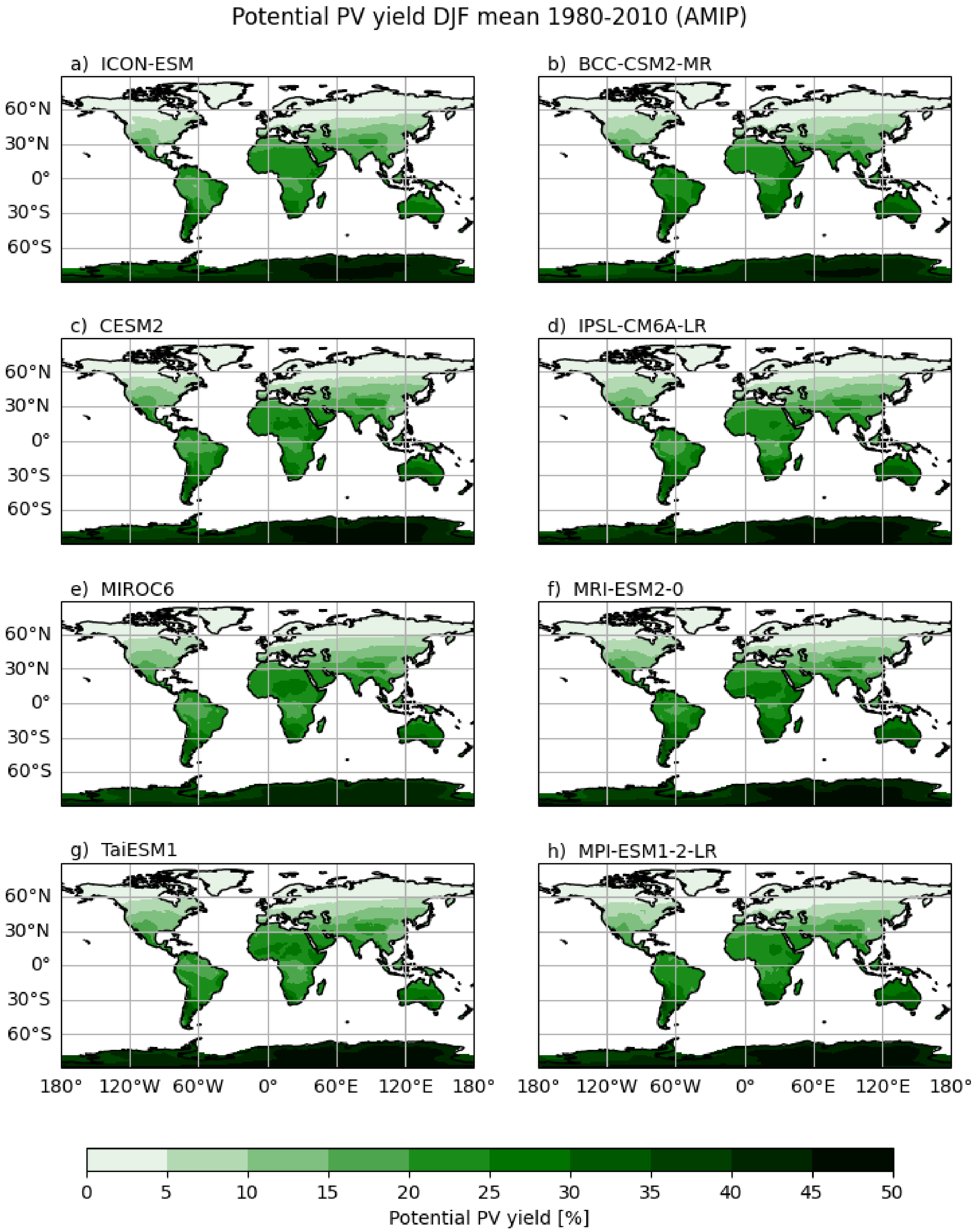

Figure 23: Mean DJF (1980-2010) potential PV yield for an ICON-ESM AMIP simulation and seven CMIP6 AMIP models.

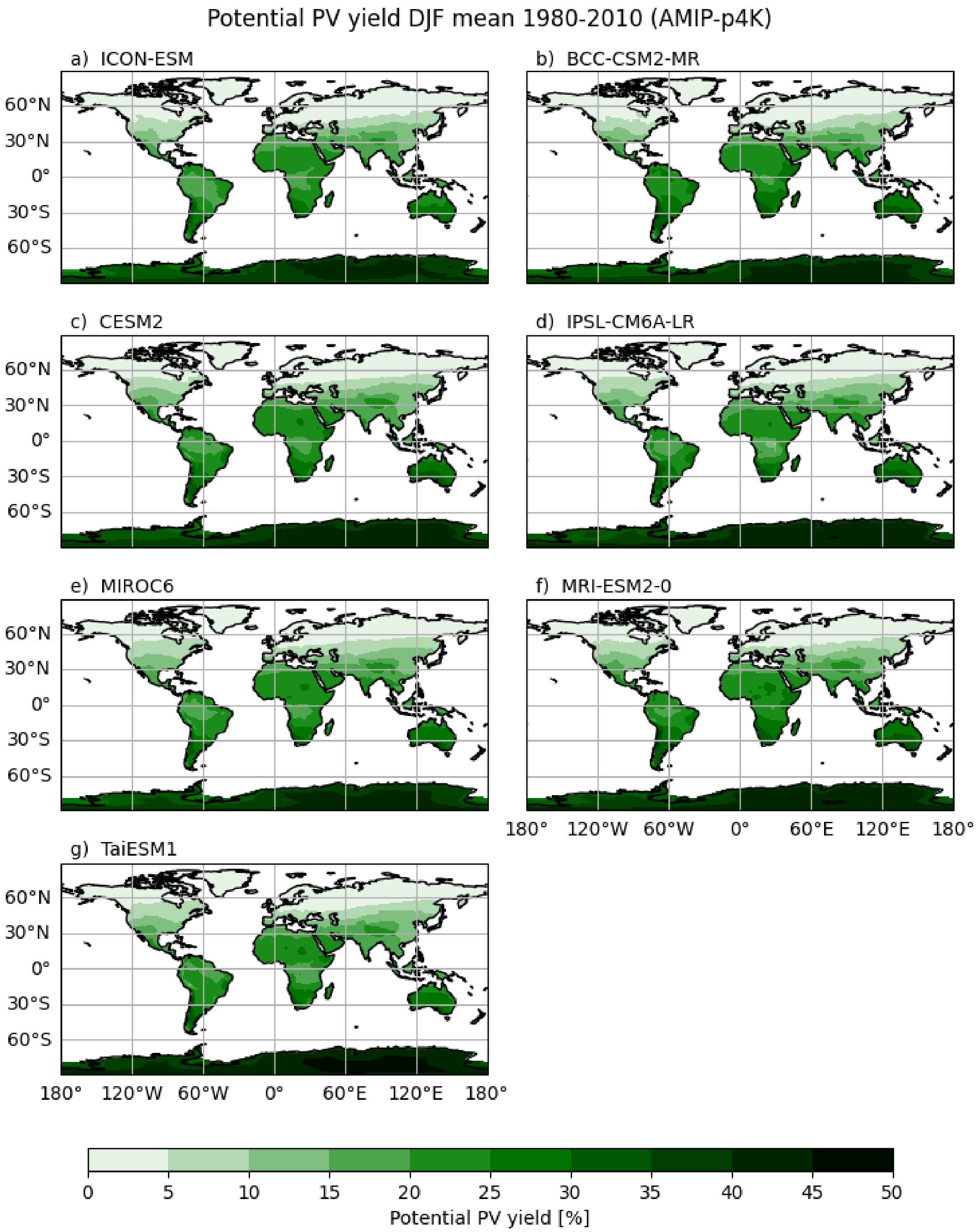

Figure 24: Mean DJF (1980-2010) potential PV yield for an ICON-ESM AMIP-p4K simulation and the six CMIP6 AMIP-p4K models.

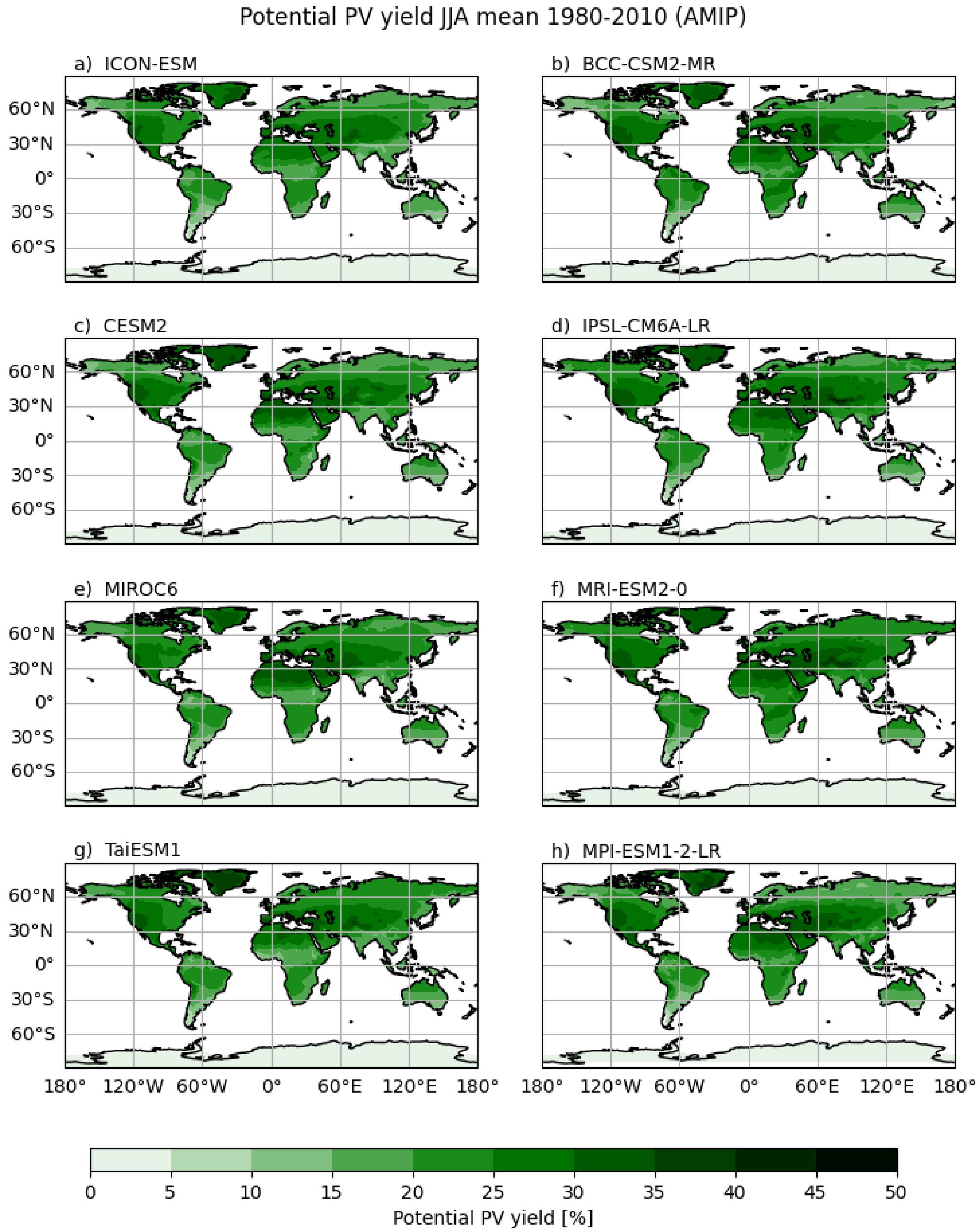

Figure 25: Mean JJA (1980-2010) potential PV yield for an ICON-ESM AMIP simulation and seven CMIP6 AMIP models.

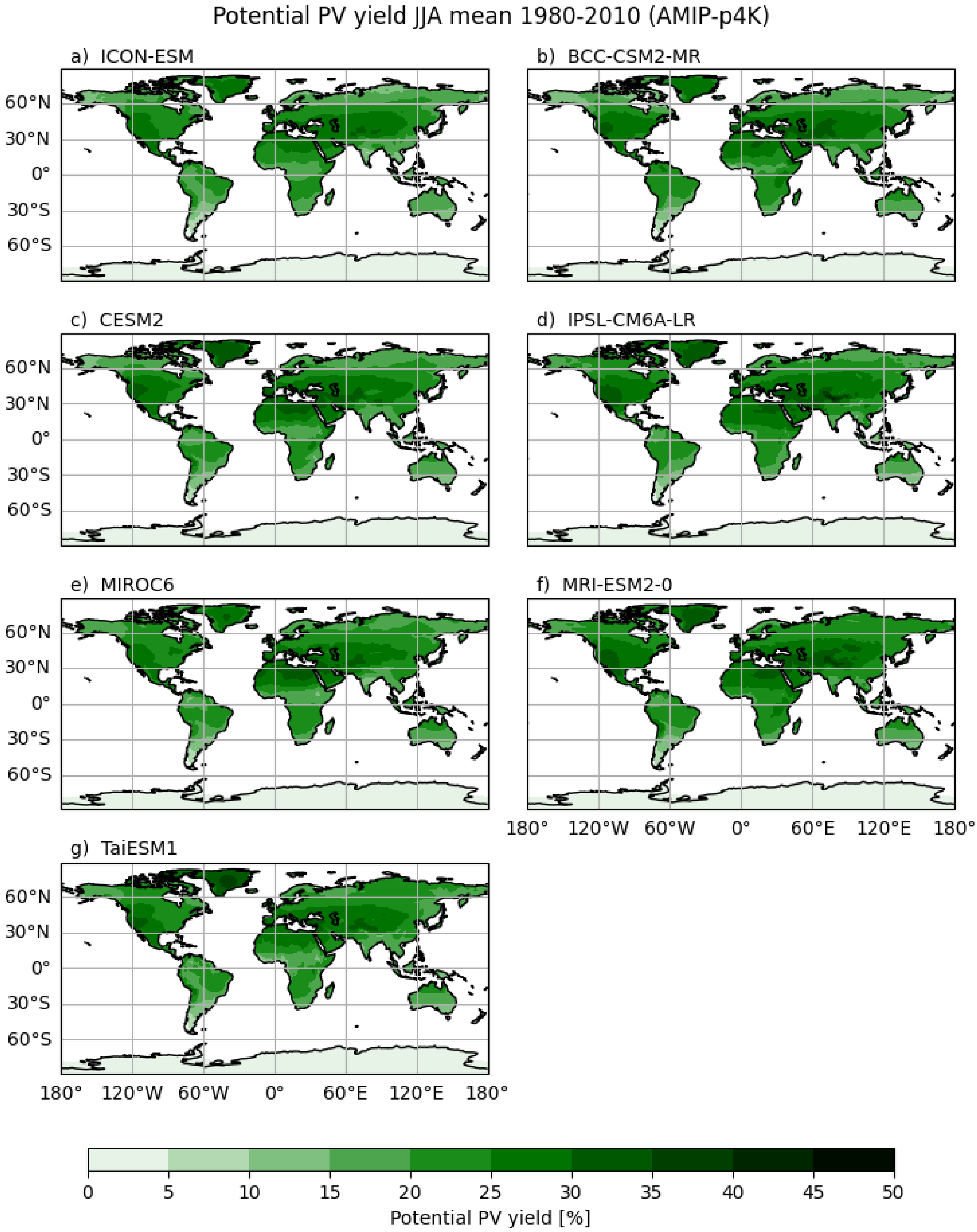

Figure 26: Mean JJA (1980-2010) potential PV yield for an ICON-ESM AMIP-p4K simulation and the six CMIP6 AMIP-p4K models.

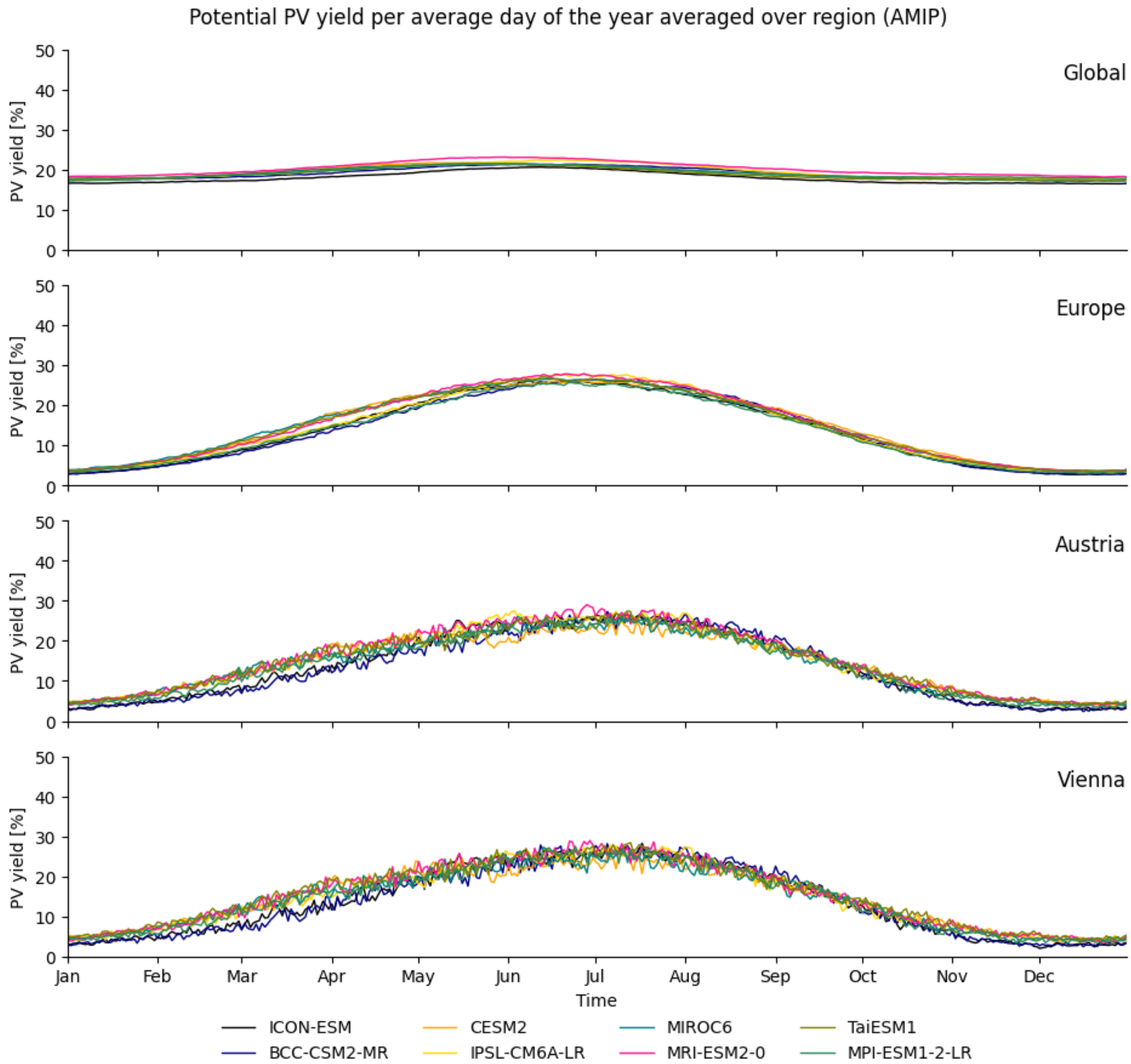

Figure 27: CMIP6 models and ICON simulation with AMIP run: time (1980-2010) and global and regional (Europe, Austria and Vienna) mean potential PV power yield in % (y-axis) per day of the year (x-axis).

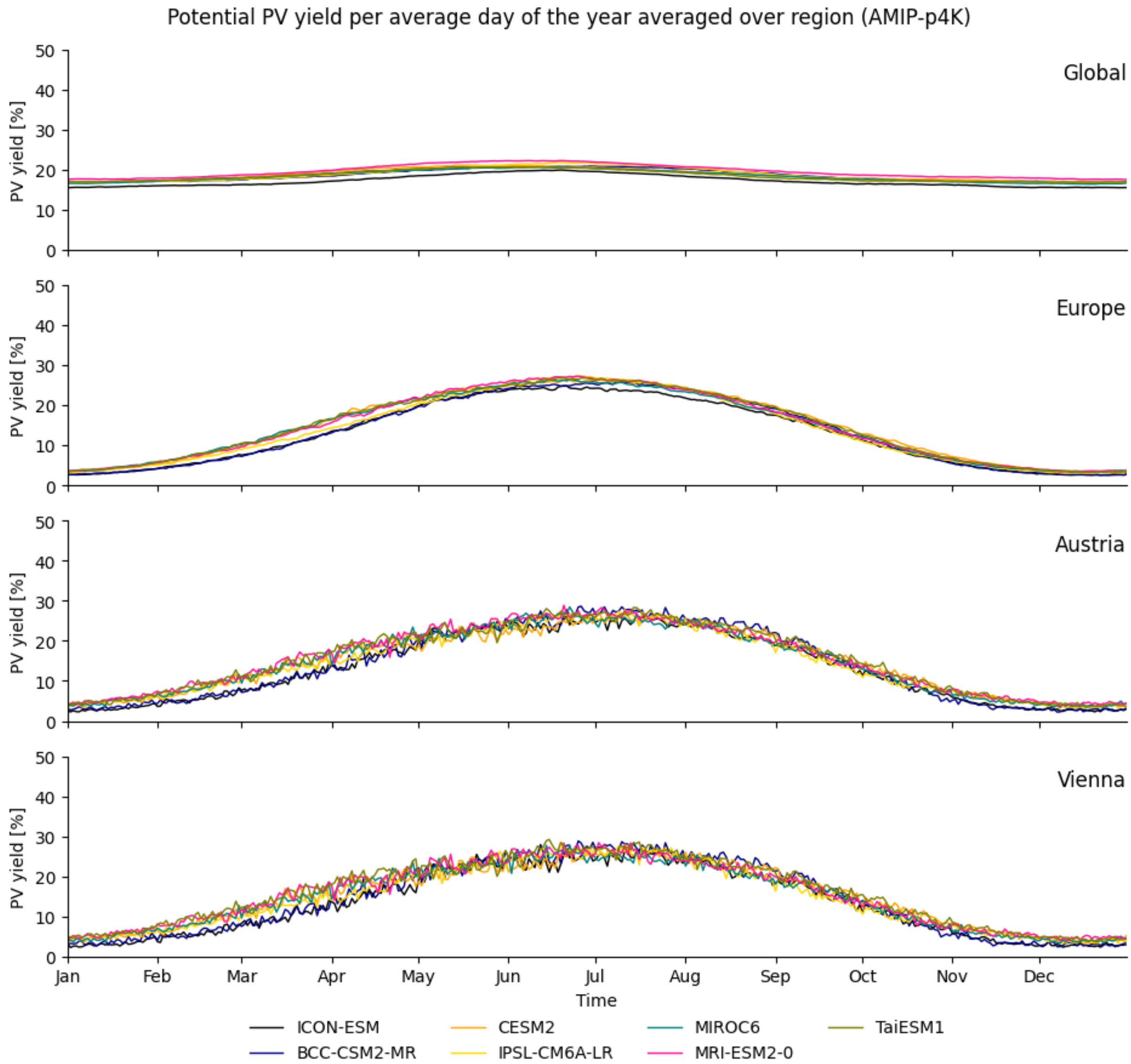

Figure 28: CMIP6 models and ICON simulation with AMIP-p4K run: time (1980-2010) and global and regional (Europe, Austria and Vienna) mean potential PV power yield in % (y-axis) per day of the year (x-axis)